5 November 2026

Structural and Climatic Controls on Forest Carbon and Water Fluxes across the Italian Alps

Vincenzo Saponaro[1], Elia Vangi[2], Anna Candotti[3], Daniela Dalmonech[4], Marta Galvagno[5], Gianluca Filippa[6], Alessio Collalti[7], Enrico Tomelleri[8]

1. Libera Universita di Bolzano Facolta di Scienze agrarie ambientali e alimentari
2. geoLAB - Laboratory of Forest Geomatics, Department of Agriculture, Food, Environment and Forestry, Università degli Studi di Firenze, Firenze, Italy;
3. Free University of Bozen-Bolzano
4. Forest Modelling Lab., Institute for Agriculture and Forestry Systems in the Mediterranean, National Research Council of Italy (CNR-ISAFOM), Perugia 06128, Italy
5. Environmental Protection Agency of Aosta Valley
6. Environmental Protection Agency of Aosta Valley
7. Consiglio Nazionale delle Ricerche
8. Free University of Bozen-Bolzano

Keywords

Process-based model, Italian Alpine forests, Machine Learning, Remote sensing, Carbon fluxes, Water Fluxes

Posted on 5 November 2026 — CC-BY-NC 4.0 — This is a preprint and has not been peer reviewed. Data may be preliminary. — https://doi.org/10.22541/essoar.15011732/v1

Structural and Climatic Controls on Forest Carbon and Water Fluxes across the Italian Alps

V. Saponaro [1,*], E. Vangi [2,3,*], A. Candotti [1], D. Dalmonech [3], M. Galvagno [4], G. Filippa [4], A. Collalti [3] and E. Tomelleri [1,5,†]

[1] Faculty of Agricultural, Environmental and Food Sciences, Free University of Bozen-Bolzano, Piazza Università/Universitätsplatz, Bolzano 39100, Italy;

[2] geoLAB - Laboratory of Forest Geomatics, Department of Agriculture, Food, Environment and Forestry, Università degli Studi di Firenze, Firenze, Italy;

[3] Modelling Lab., Institute for Agriculture and Forestry Systems in the Mediterranean, National Research Council of Italy (CNR-ISAFOM), Perugia, Italy;

[4] Environmental Protection Agency of Aosta Valley, Climate Change Unit, ARPA Valle d'Aosta, Italy;

[5] Competence Centre for Mountain Innovation Ecosystems, Free University of Bozen-Bolzano, Italy.

Corresponding author: Vincenzo Saponaro (vincenzo.saponaro@unibz.it)

* **Equally contributed**

† **Deceased**

Key Points:

- Estimating carbon and water fluxes across mountain landscapes remains a major challenge due to their high environmental heterogeneity.
- We combined forest and hydrological models with remote sensing and four machine learning algorithms to estimate carbon and water fluxes.
- Created high-resolution maps for gross primary productivity, net primary productivity, and evapotranspiration across Italian Alpine forests.

Abstract

Estimating carbon and water fluxes across mountain landscapes is challenging due to environmental heterogeneity. In the Italian Alps, complex topography and fragmented land use further complicates carbon accounting. The European Green Deal recognizes forests as climate allies, requiring accurate, spatially explicit assessments of their carbon and water exchange. To address this pressing need, we first simulated carbon and water fluxes of the Italian National Forest Inventory plots using a process-based ecosystem model. These simulations, together with predictors derived from remote sensing and a hydroclimatic model, were used to train four machine learning algorithms. We developed an integrated framework combining the process-based model with these data-driven methods to generate 30m resolution maps of Gross Primary Productivity (GPP), Net Primary Productivity (NPP), and Evapotranspiration (ET) across the Italian Alps for 2020. Among the tested models, Random Forest consistently achieved the highest predictive performance. Biomass predictors mainly explained GPP and NPP, climate controlled ET. The results (R^2 = 0.40, 0.28, and 0.27 for GPP, NPP, and ET, respectively) provide valuable insights into the complexity and spatial heterogeneity of Alpine forest ecosystems, highlighting the complementary information captured by integrated modelling approaches. Our results demonstrate the potential of integrated modelling to generate spatially explicit estimates of forest carbon and water fluxes, offering additional perspectives on ecosystem functioning beyond those captured by individual observational datasets. The resulting maps provide unprecedented spatial detail for GPP, NPP, and ET across Italian Alpine forests, supporting ecosystem monitoring, carbon budget assessments, and forest management strategies for climate adaptation and mitigation.

Plain Language Summary

Forest ecosystems play an important role in removing carbon dioxide from the atmosphere and storing carbon in vegetation and soils. They also regulate water cycling, which can influence local and regional climate conditions. These mechanisms are increasingly important because human activities, particularly the burning of fossil fuels, are raising atmospheric carbon dioxide concentrations and contributing to climate change. However, estimating carbon and water fluxes across the Italian Alps is challenging. The region includes strong environmental gradients, diverse forest types, fragmented land use, different management practices, and several administrative boundaries. These factors make it difficult to produce consistent estimates over large areas. To address this challenge, we developed a framework that combines a process-based ecosystem model, an hydroclimatic model, satellite observations, and machine-learning algorithms. Together, these tools allow us to estimate forest carbon and water fluxes at high spatial resolution. The framework produces continuous maps of gross primary productivity, net primary productivity, and evapotranspiration across the Italian Alps. These maps can support ecosystem monitoring, improve regional carbon-budget assessments, and inform forest-management strategies for climate-change mitigation and adaptation.

1 Introduction

According to the IPCC (2022), the Paris Agreement (2015) and subsequently the Glasgow climate conference (COP26, 2021), limiting global warming to 1.5°C – or well below 2°C – above pre-industrial levels requires achieving a balance between anthropogenic emissions and removals (i.e., net-zero CO_2e emissions) by the second half of this century. The European Green Deal (European Commission, 2021) highlights the crucial role of forests as key allies in both adapting to and fighting climate change. To this purpose, forest ecosystems play a vital role in absorbing carbon dioxide from the atmosphere and storing it in their tissues (Lorenz & Lal, 2009), as well as in the soil (Lal, 2005). However, across the biomes, not all ecosystems have the same capacity to absorb and store atmospheric carbon dioxide, as this process is influenced by environmental variables, topography, species composition, forest age, anthropogenic and natural disturbances (Holtmann et al., 2021; Migliavacca et al., 2021; Saponaro et al., 2025; Vangi et al., 2024). This is particularly true in Alpine regions, where both the physical landscape, characterized by complex terrain, diverse ecosystems, and fragmented land use, and administrative complexity pose unique challenges for coherent climate policy and carbon accounting (Food and Agriculture Organization of the United Nations et al., 2019; Kotlarski et al., 2022). Europe, and the European Alps in particular, are considered especially vulnerable to climate change, which can alter forest structure and species composition, thereby driving substantial changes in carbon and water fluxes and making them increasingly difficult to quantify accurately (Bonan, 2008; Frank et al., 2015; Rank et al., 2023). This could weaken the forest's carbon sequestration and long-term carbon sink capacity (Alsafadi et al., 2024; Hartmann et al., 2022). In addition, the frequent snow droughts, declining snow cover and glacier retreat in the Alps are expected to severely limit tree water availability (Avanzi et al., 2024; Brighenti et al., 2024; Gobiet et al., 2014). Furthermore, alterations in precipitation regimes (e.g. dry spells) associated with climate change, together with rising temperatures, are expected to increase atmospheric vapor pressure deficit (VPD), thereby enhancing atmospheric evaporative demand and intensifying water loss from forest ecosystems (Karimzadeh et al., 2025; Khadke et al., 2026; Schönbeck et al., 2022). Forests and understory vegetation strongly regulate the water cycle through transpiration (T), which is one of the major fluxes alongside evaporation from the soil (E), in which the combination is known as Evapotranspiration (ET)

(Sheil, 2018; Thornthwaite & Mather, 1951). Transpiration is regulated via stomatal conductance, which in turn depends on hydraulic root conductivity of the plant, soil moisture, solar radiation, leaf CO_2 concentration, and VPD (Bonan et al., 2014; Jarvis, 1976; Whitehead, 1998). Nearly 40% of global terrestrial precipitation is taken up by plant roots and returned to the atmosphere as water vapor via stomatal transpiration, which rises significantly when accounting for direct soil evaporation and canopy interception (Schlesinger & Jasechko, 2014). Accurately estimating ET in the Alpine ecosystem is crucial not only for forest water resource management and climate change impact assessments, but also for understanding forest water regulation and the strong land-atmosphere coupling that characterizes these mountain environments.

In the context of carbon accounting, many countries have established a system of measurement known as National Forest Inventories (NFI) to track the stocks of wood and carbon, which in the past were more oriented to biomass production, and later evolved to monitor also biodiversity, disturbances, ecosystem service functions (e.g. freshwater, biomass, food, soil formation and so on) as well as climate change impacts (Araza et al., 2023).

Traditional NFIs rely on a field network of sampling points (i.e., forest plots) in which qualitative and quantitative attributes are measured periodically. Field surveys are processed to provide aggregated statistics at different administrative levels (usually from national to NUTS2 level). However, traditional NFIs suffer from sparse sampling and long survey cycles (usually from 5 to 10 years), which are not able to fulfil the periodic international reporting needs and the operational decision-making at the single-owner level. To augment traditional NFI, forest models provide a complementary framework for estimating dynamic ecosystem variables and for projecting long-term changes in stand structure (Liu et al., 2022; Morales et al., 2005; Morichetti et al., 2024). By integrating structural forest stand data from the NFI with climatic inputs, stand level process-based models can be used to simulate carbon and water fluxes, as well as their temporal dynamics. This approach enables the use of contemporary and future projections to determine whether forests act as carbon sinks or sources (Härkönen et al., 2011). However, although process-based models are essential for representing key ecological processes (Niu et al., 2021), they may be constrained by parameter uncertainty and process representations (Larocque et al., 2008; Shiklomanov et al., 2020). In this regard, combining them with complementary data and approaches, including remote sensing (RS) products and machine learning (ML) algorithms, can enhance the overall accuracy and interpretability of simulations (Boukhris et al., 2025; Dou et al., 2018).

Adopting a hybrid framework that leverages ML algorithms and RS data is necessary to bridge the gap between site-specific data and landscape-level estimations, as already explored by Jung et al. (2011) and Maxwell et al. (2018). This approach moves beyond the constraints of traditional parametric relationships, enabling robust spatial upscaling by accounting for the complex, multi-dimensional interactions within forest ecosystem functioning datasets.

To better understand and quantify the role of Italian Alpine forests to regional carbon and water budgets, this study estimates their contributions to these fluxes. Forest carbon and water fluxes were predicted using a multi-approach framework: first, by simulating NFI field plots of the forest stand distributed across the entire Italian Alpine region, and then by integrating RS data with ML algorithms to spatialize the results and produce a high-resolution (30 m) wall-to-wall map of the region.

In this respect, it is crucial to perform a high-resolution analysis of the spatial variability of Alpine forest responses, specifically regarding Gross Primary Production (GPP), Net Primary Production (NPP), and Evapotranspiration (ET).

Specifically, we aimed, for the first time for the Italian country, to: (i) generate spatially continuous 30 meters estimates of GPP, NPP, and ET for the test-year 2020; (ii) identify the relative importance (i.e. permutation importance) of forest structural, climatic, topographic, and phenological variables in explaining the spatial variability of these fluxes; and (iii) quantify the uncertainty associated with the resulting spatial predictions. We hypothesised that carbon and water fluxes would respond to fundamentally different environmental controls: (H1) spatial variation in GPP and NPP would be primarily shaped by forest structure, with greater canopy development and biomass supporting higher carbon assimilation; whereas (H2) ET would be governed more strongly by climate and moisture availability, reflecting the predominant control of atmospheric demand and water supply over ecosystem water fluxes.

2 Materials and Methods

2.1 Study area

157 The Italian Alpine region spans approximately 52,000 km² across seven administrative
158 regions, extending from Valle d'Aosta in the west to Friuli Venezia Giulia in the east. This
159 area exhibits substantial topographic variability, encompassing elevations ranging from
160 1,386 m a.s.l. (Monte Settepani) to 4,810 m a.s.l. (Monte Bianco). At the regional scale,
161 the northwestern and northeastern sectors of the Greater Alpine Region (GAR) display a
162 broadly coherent warming signal (+1.1-1.6°C per century). The precipitation signal varies
163 significantly across regions and altitudes, with winter precipitation increasing in the
164 northwestern Alps (+20% to +40% per century), while summer brings widespread drying
165 (e.g. dropping by 20%–30% per century in western plains and 40%-50% per century in
166 the southern plains), compared to a minor decline (<10%) above 1500 m (Brunetti et al.,
167 2006, 2009; Ménégoz et al., 2020). In the Italian Alpine region, forest composition varies
168 with altitude: lower montane zones are dominated by broadleaf species such as
169 European beech (*Fagus sylvatica* L.), sessile oak (*Quercus petraea* (Matt.) Liebl.),
170 pedunculate oak (*Quercus robur L.*), pubescent oak (*Quercus pubescens* Willd.), and
171 chestnut (*Castanea sativa* Mill.), whereas mid-to-upper montane belts are characterized
172 by mixed and pure stands of norway spruce (*Picea abies* (L.) H. Karst), silver fir (*Abies*
173 *alba* Mill.), European larch (*Larix decidua* L.), scots pine (*Pinus sylvestris* L.), Swiss stone
174 pine (*Pinus cembra* L.), and mountain pine (*Pinus mugo* Turra).

175 ## 2.2 Data description

176 ### 2.2.1 National Forest Inventory data

Field data were collected as part of the third Italian NFI (INFC, 2015). The Italian NFI employed a systematic, unaligned sampling design based on a 1 km x 1 km grid of temporary plots, conducted in three distinct phases (Fattorini et al., 2006). In the first phase, each sampling point was photo-interpreted to classify land use. During the second phase, qualitative field data were collected from a subset of points identified as forested. This information included silvicultural and management systems, forest category, ownership, constraints, and accessibility. In the third phase, a total of 6,174 points from the second phase were selected, stratified by administrative regions (NUTS2 level) and forest types. At these locations, quantitative data were collected within 13-meter radius circular plots, including tree species, diameter at breast height (DBH), and tree height, which were used to calculate the growing stock volume (GSV) for each callipered tree using national species-specific allometric models (Tabacchi et al., 2011). Plot-level GSV was derived by aggregating tree-level GSV. The third-phase field survey was carried out between 2018 and 2020. Recently, Vangi et al. (2025) performed the first National-scale simulation and validation of the 3D-CMCC-FEM process model (see supplementary materials for a description of the model and 2.2.2 for the model setup), using third-phase data from the second and third Italian NFI (field surveys carried out in 2005 and 2015, respectively), demonstrating the model's ability to accurately predict carbon stocks and fluxes. In this study, plot-level data resulting from those simulations were used. All plots in the Alpine region were selected, totaling 1516 plots (Fig. 1), for which values of carbon and water fluxes, as well as modelled biomass and carbon stocks, are available for the years 2005-2020. Moreover, disturbed plots were identified and removed, yielding a final dataset of around 1415 plots. For a complete list of the model variables available in the selected plots, refer to Vangi et al. (2025) and Collalti et al. (2024).

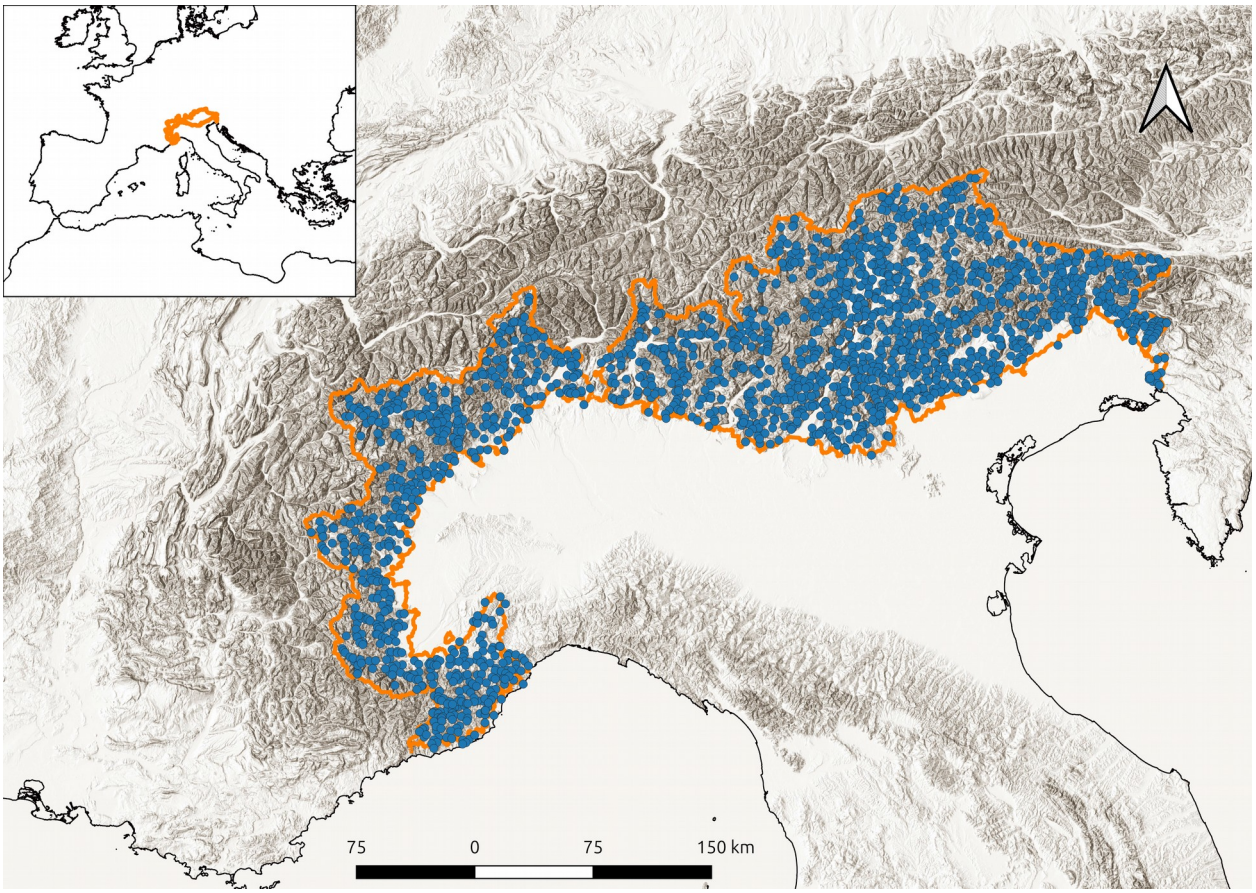


Fig. 1. Study area (in orange) and spatial distribution of the NFI plots within the study area (blue points).

2.2.2 Process-based model output data

The 3D-CMCC-FEM (*Three Dimensional - Coupled Model Carbon Cycle - Forest Ecosystem Module*; Collalti et al., 2016, 2024; Dalmonech et al., 2026; Marconi et al., 2017; Morichetti et al., 2024) simulations used in this study were performed by Vangi et al. (2025), using approximately 5135 Italian NFI plots. The model was initialized in 2005, corresponding to the second NFI field campaign, using the stand characteristics recorded during that survey, and was run until 2020, corresponding to the third Italian NFI field campaign. Since the simulated points from Vangi et al. (2025) covered the entire Italian national territory, we selected only those located within our study area, the Italian Alpine region (Fig.1). A comprehensive description of how carbon and water fluxes are simulated by the 3D-CMCC-FEM model is provided in the supplementary materials and in Collalti et al. (2024).

2.2.3 Spatial predictor variables

2.2.3.1 Vegetation phenology and productivity

High-Resolution Vegetation Productivity and Phenology (HRVPP) is a new suite of products from the Copernicus Land Monitoring Service (CLMS), including Vegetation Phenology Parameters (VPP), generated annually from the seasonal trajectory of the Plant Productivity Index derived from Sentinel-2 time. VPP comprises 13 phenology metrics that describe vegetation dynamics during the growing season. For a more in-depth description of the HRVPP suite, refer to Vangi et al. (2026).

2.2.3.2 Forest structure and composition

The forest GSV map for the study region was obtained by combining field observation with RS data. Field reference data were derived from 4,877 plots surveyed within the Italian NFI (INFC, 2015). We used all field plots excluding those located within the Italian Alps study area to avoid imposing an artificial correlation between the dependent variables and the predictors. To be consistent with the reference year of the study, we selected only plots measured between 2019 and 2020. RS predictors were derived from national Sentinel-2 composites obtained with the Best Available Pixel approach (White et al., 2014). We expanded the original spectral bands (blue, green, red, red-edge 1–4, NIR, SWIR1, SWIR2) by calculating several vegetation indices: normalized difference vegetation index (NDVI), normalized burn ratio (NBR), enhanced vegetation index (EVI), and Tasseled Cap Brightness (TCB), Wetness (TCW), Greenness (TCG), and Angle (TCA). Based on these 13 variables, harmonic metrics were computed following Shumway and Stoffer (2017). For each pixel, four harmonic coefficients were estimated, together with amplitude, phase, and root mean square error (RMSE), resulting in 91 harmonic metrics. To benchmark harmonic predictors, we also generated four seasonal cloud-free composites (autumn, winter, spring, and summer) using the Medoid compositing approach (Kennedy et al., 2010), which selects pixels with reflectance values closest to the temporal median of the image collection. Additional predictors included elevation, slope, aspect, and spatial coordinates. We used the random forest (RF) algorithm to model the relationship between measured GSV and RS predictors. Hyperparameters were optimized using leave-one-out cross-validation (LOOCV), testing all combinations of variables used for splitting (mtry = 10–50), number of trees (ntree = 200, 500, 1000), and minimum node size (min.node.size = 1, 3, 5, 10, 20), for a total of 615 runs. The best model, selected according to the highest coefficient of determination (R^2), was finally applied to map GSV across the Italian Alps.

The gridded above-ground biomass (AGB) dataset was computed by integrating Alpha Earth Foundation (AEF) Satellite Embeddings and GEDI-derived AGB estimates (Candotti & Tomelleri, 2026). The AEF embeddings represent numerical and unitless temporal and geographical interactions extracted as embeddings between important planetary variables detected in Earth Observation missions, which result in 64 dimensions (bands) at a 10-m native spatial resolution (Brown et al., 2025). Embeddings from the year 2022 were selected. GEDI-derived AGB estimates of the same year are available at a 25-m spatial resolution from the GEDI L4R Raster AGB density (Mg/ha) dataset (Dubayah et al., 2022). A RF regression model was chosen to predict AGB for the alpine region at a common 30 m spatial resolution, using a subset of 3000 GEDI AGB estimates. The calculations were performed in the Google Earth Engine (GEE) computing platform. To measure the goodness, standard performance statistics such as absolute values for RMSE and Pearson's correlation (R) between predicted and GEDI-derived AGB were extracted. Independent comparisons were performed with AGB from the Italian NFI and from ESA's Climate Change Initiative (CCI Biomass). The canopy height model (CHM) was considered using the dataset provided by Tolan et al. (2024). Covering the period from 2019 to 2020, this 1 m resolution global dataset provides a global analysis of tree height and occupancy. The Tolan CHM was selected due to its direct temporal alignment with the study period. Before using the CHM data for our purpose, we regridded the spatial resolution from 1 m to 30 m. The LAI was obtained from CLMS using Sentinel-3 imagery from May to September 2020. The index was derived using the 10-day images, and processed via Climate Data Operators (CDO) (Schulzweida, 2023) to generate a median composite for the study area (CLMS, 2017, accessed 04/2026). To account for forest composition, we integrated the European tree genus map (hereafter indicated as "Species") at 10 m resolution, then resampled at 30 m resolution, for the year 2020 (De Keersmaecker et al., 2024). This dataset, derived from Sentinel-1 and Sentinel-2 imagery, provides a detailed classification of eight dominant taxa, including Larix, Picea, Pinus, Fagus, and Quercus, allowing for genus-specific analysis of ecosystem fluxes (accessed 02/2026).

2.2.3.3 Climatic drivers

High-resolution climate data, including temperature (Temperature), precipitation (Precipitation), radiation (Radiation), relative humidity (Relative_hum), wind speed (Wind_speed), snow water equivalent (SWE) and snow depth (SNOWDPTH), were simulated using the physically based snow-hydrological model openAMUNDSEN v1.0.0 (Alpine MUltiscale Numerical Distributed Simulation Engine). This model, specifically developed for mountain environments, incorporates spatial interpolation of meteorological observations while accounting for complex topographic effects (Strasser et al., 2024). Model simulations were driven by ERA5 reanalysis data across the Alpine region, where more than 100 data points were selected to serve as local thermopluviometric reference stations (C3S, 2018). These data, comprising air temperature, precipitation, solar radiation, relative humidity and wind speed, were used to force the model at a spatial resolution of 30 m and a daily temporal resolution. In addition, we calculated VPD from the relative humidity simulated by openAMUNDSEN for the same year using Teten's equation (Tetens, 1930) and processed via CDO.

2.2.3.4 Topographic and other predictors

296 The National Digital Elevation Model (DEM) from the TINITALY project with a spatial
297 resolution of 10 m, is currently the finest-resolution DEM available at the national level
298 (Tarquini et al., 2007). From the DEM, slope and aspect were derived using the Horn
299 formula (accessed 03/2025). The aspect was then further subdivided into Northness and
300 Eastness using sine and cosine trigonometric calculations to obtain greater ecological
301 information as a predictor. The High-resolution Layer Forest Type (FTY) was retrieved
302 from the Copernicus database (2018-present) at 10 m spatial resolution, which provides
303 information on pan-European forests. The FTY is divided into three classes: all non-forest
304 areas, broadleaved forest, and coniferous forest. The map is first regridded to match the
305 common 30 m spatial resolution of all other variables and then used as a forest mask
306 during the analysis (EEA 2024, accessed 08/2025). The Enhanced Vegetation Index 2
307 (EVI2) was calculated using Sentinel-2 L2A harmonized imagery from May to September
308 2020. The index was derived using a two-band approach, near-infrared (B8) and red (B4)
309 bands, and processed via GEE to generate a cloud-masked median composite for the
310 study area
311 (https://developers.google.com/earth-engine/datasets/catalog/COPERNICUS_S2_SR_HA
312 RMONIZED, accessed 03/2026). Land Surface Temperature (LST) for 2020 was retrieved
313 from Landsat 8 Collection 2 Level-2 imagery for the period May-September. The
314 processing workflow involved atmospheric correction using internal scaling factors,
315 cloud masking, and the derivation of land surface emissivity based on the Fractional
316 Vegetation Cover (FVC) method. Also in this case LST values were calculated using GEE
317 (https://developers.google.com/earth-engine/datasets/catalog/LANDSAT_LC08_C02_T1
318 _L2#terms-of-use, accessed 01/2026). To account for vegetation-soil water content, the
319 Normalized Difference Moisture Index (NDMI) was calculated using Sentinel-2 L2A
320 imagery. Following Gao B.C. (1996), the index was derived from the near-infrared (B8)
321 and short-wave infrared (B11) bands. A seasonal mean composite was generated for the
322 period between May and September 2020 to avoid the snow signal, applying a bitwise
323 cloud mask to the QA60 band to ensure data quality and minimize atmospheric
324 interference

(https://developers.google.com/earth-engine/datasets/catalog/COPERNICUS_S2_SR_HARMONIZED#bands, accessed 11/2025). To derive the Snow Cover Duration (SCD) for the year 2020, we processed daily fractional snow cover (FSC) data, provided by the Copernicus Land Monitoring Service, using CDO. The daily observations were first concatenated into a continuous annual time series. Subsequently, a binary snow mask was generated by thresholding the pixels to isolate snow presence. Finally, the SCD was calculated by performing a temporal summation of the masked daily values, yielding the total number of snow-covered days per pixel for the entire year (accessed 04/2026). A brief list of all products is provided in Table 1, whereas a complete list is in Table S1.

Table 1. The brief list of the 35 predictors available for use as input for the machine learning algorithms. All the predictors were obtained for 2020.

Predictors	
Category	**Abbreviation**
Vegetation phenology and productivity	AMPL – EOSD – EOSV – LEGHT – LSLOPE – MAXD – MAXV – MINV – RSLOPE – SOSD – SOSV – SPROD – TCW – TPROD
Forest structure and composition	GSV – AGB – CHM – LAI – Species
Climate drivers	Precipitation – Radiation – Relative_hum – Temperature – Wind_speed – SWE – SNOWDPTH – VPD
Topographic and other environmental predictors	DEM – Slope – Northness – Eastness – EVI2 – LST – NDMI – SCD

336

337 2.2.4 Machine-learning models

338 We evaluated four ML algorithms, Random Forests (RF), Extreme Gradient Boosting
339 (XGB), Support Vector Machine (SVM), and Artificial Neural Network (ANN), to predict
340 key forest variables, GPP, NPP and ET. The RF is an ensemble-tree algorithm that has
341 shown strong performance in capturing complex, nonlinear relationships (Breiman,
342 2001; Pagano et al., 2023), while being robust to overfitting and collinearity among
343 predictors. XGB is a supervised learning algorithm based on a scalable, end-to-end tree-
344 boosting system. Like RF, XGB is an ensemble of decision trees, but it uses gradient-
345 based optimization to build the ensemble, sequentially training weak learners to
346 improve the previous models' performance (T. Chen & Guestrin, 2016). Here we used
347 the following parameterization, with 500 trees (n_estimator), a tree depth of 3
348 (max_depth) and a learning rate of 0.1.

The SVM can generate non-linear decision surfaces by mapping the data into a high-dimensional space via nonlinear mapping functions called kernel functions (Cortes & Vapnik, 1995; Pal & Mather, 2005), allowing the data to be separated by linear hyperplanes (Dixon & Candade, 2008). In this study, we employed Support Vector Regression (SVR) with a C of 500 and ε of 0.1. ANNs are computational models biologically inspired by the structure of the human brain, consisting of a dense network of interconnected nodes (neurons) that process information through weighted connections (Mehrotra et al., 1997). Specifically, we used the Multi-layer Perceptron (MLP) regression, a supervised learning algorithm trained via backpropagation. To handle non-linear dependencies, we implemented a regressor consisting of two hidden layers with 64 neurons each. We set the Rectified Linear Unit (ReLU) activation function and the solver "Adam" (Kingma & Ba, 2014). The model was configured with a maximum of 1000 iterations to ensure sufficient convergence time; however, to prioritize generalization and prevent overfitting, an early stopping mechanism was integrated, terminating the training process if the validation loss failed to improve for 20 consecutive iterations. To ensure robust evaluation and control for spatial autocorrelation, we applied 5-fold cross-validation together with a group spatial block analysis for each algorithm. The analyses were performed using Python v.3.13.9. The predictive accuracy and performance of the machine learning algorithms for GPP, NPP, and ET were evaluated using the R^2, RMSE, and relative RMSE (RMSE%).

Importantly, after comparing the performance of the four ML algorithms, we selected RF to generate the wall-to-wall maps and for all subsequent analyses (section 2.2.5) because it achieved the highest predictive performance.

2.2.5 Model optimization and interpretation

2.2.5.1 Recursive Feature Elimination with Cross-Validation

Before running the RF algorithm for each of the target variables, we performed a feature selection algorithm, as also used by Barzani et al. (2024). The Recursive Feature Elimination with Cross-Validation (RFECV) is a useful technique for identifying the most relevant features to optimize model performance and interpretability. The RFECV was implemented using an RF regressor as the underlying estimator. This estimator was configured with 100 decision trees (n_estimators=100) and a fixed random_state=0 to ensure result reproducibility. The selection process followed a step-wise pruning approach, where one feature was removed at each iteration (step=1) based on its importance rank. To ensure the stability and generalizability of the selected subset, a 5-fold Cross-Validation strategy with shuffling (KFold, n_splits=5) was considered. The optimal number of features was determined by maximizing the R^2 score, ensuring that the final subset retained the highest predictive power for the continuous GPP, NPP and ET target variables.

2.2.5.2 Hyperparameter tuning

Following the feature selection process, the RF model was further refined through hyperparameter optimization. To identify the optimal model configuration, we performed hyperparameter tuning using the *RandomizedSearchCV* function (Scikit-learn Python package) across 30 iterations. The research comprises critical parameters including the number of estimators, maximum tree depth, minimum samples per leaf, and maximum features. The best combination was selected based on the R^2 score, evaluated through a 5-fold cross-validation strategy to identify the configuration that yielded the highest predictive accuracy for the target variables.

2.2.5.3 Permutation importance

Once the RF model was fitted to the entire dataset, permutation importance was utilized to evaluate feature contributions. The method relies on the repeated permutation of a feature to break its relationship with the target variable (i.e. GPP, NPP and ET), allowing for an estimation of the resulting importance scores. A significant decrease in model performance following this shuffling indicates that the feature, and its original association with the outcome, is highly influential in the model's predictive process (Altmann et al., 2010). The configuration involved 30 random shuffles per predictor, using the validation subset to assess the model's generalization error. This setup allowed for a reliable quantification of each variable's impact on the model's ability to predict GPP, NPP, and ET.

2.2.5.4 Partial Dependence Plots

To interpret the complex relationships within the RF model, we utilized Partial Dependence Plots (PDP). These plots visualize the functional dependence of the target response on individual predictors, revealing the underlying patterns of interaction and the degree of non-linearity inherent in the model's decision-making process (Danesh et al., 2022).

2.2.5.5 Uncertainty quantification

To provide statistically rigorous uncertainty quantification for GPP, NPP, and ET estimates, we implemented Conformal Prediction (CP) (Angelopoulos & Bates, 2021). We leveraged CP to complement our RF model, moving beyond point estimates to provide distribution-free uncertainty intervals. By defining a 95% confidence threshold, we produced prediction sets that maintain non-asymptotic validity, offering a robust measure of reliability for the flux predictions. To implement CP, we utilized the Model Agnostic Prediction Interval Estimator (MAPIE) library in Python. Specifically, we utilized Cross-Conformal Regression (*cv=5*) with a 5-fold cross-validation scheme and the *plus* method (Taquet et al., 2022; Vovk, 2012). This configuration allowed us to generate distribution-free prediction intervals at a 95% confidence level, as mentioned before, ensuring robust uncertainty quantification for GPP, NPP, and ET estimates.

3 Results

3.1 High-resolution maps

Table 2 summarizes the performance metrics, R^2, RMSE and RMSE%, used to evaluate the predictive accuracy and performance of the ML algorithms for GPP, NPP, and ET. The four trained models were applied for the test-year 2020, where the RF outperformed the other ML algorithms, SVM achieved relatively good performance, followed by the XGB, whereas the worst performance was obtained by the ANN. Because the RF algorithm outperformed the others, we used it exclusively, as mentioned above, to generate the GPP, NPP, and ET maps (Figs. 2-3-4). The RF algorithm accurately predicted the value of GPP over the entire area of Italian Alps for the year 2020 estimating the mean value of 1460 gC m^{-2} yr^{-1}, with a minimum and maximum values of 353 and 2314 gC m^{-2} yr^{-1}, respectively (Fig.2). The highest GPP values were observed in the northeastern Alps, particularly within the Trentino-Alto Adige region, where a clear spatial pattern is evident. For the same year, the predicted NPP mean value was 630 gC m^{-2} yr^{-1}, the minimum value 177 gC m^{-2} $yr^{-1,}$ and the maximum value 1067 gC m^{-2} yr^{-1} (Fig.3). Unlike GPP, NPP displayed a more widespread distribution, showing less localized clustering along the main valleys. Lastly, predicted ET averaged 784 mm with minimum and maximum values of 135 and 1664 mm, respectively (Fig.4). ET exhibited a more uniform and widespread spatial distribution, with high values consistently occurring across most of the forested Alpine belt.

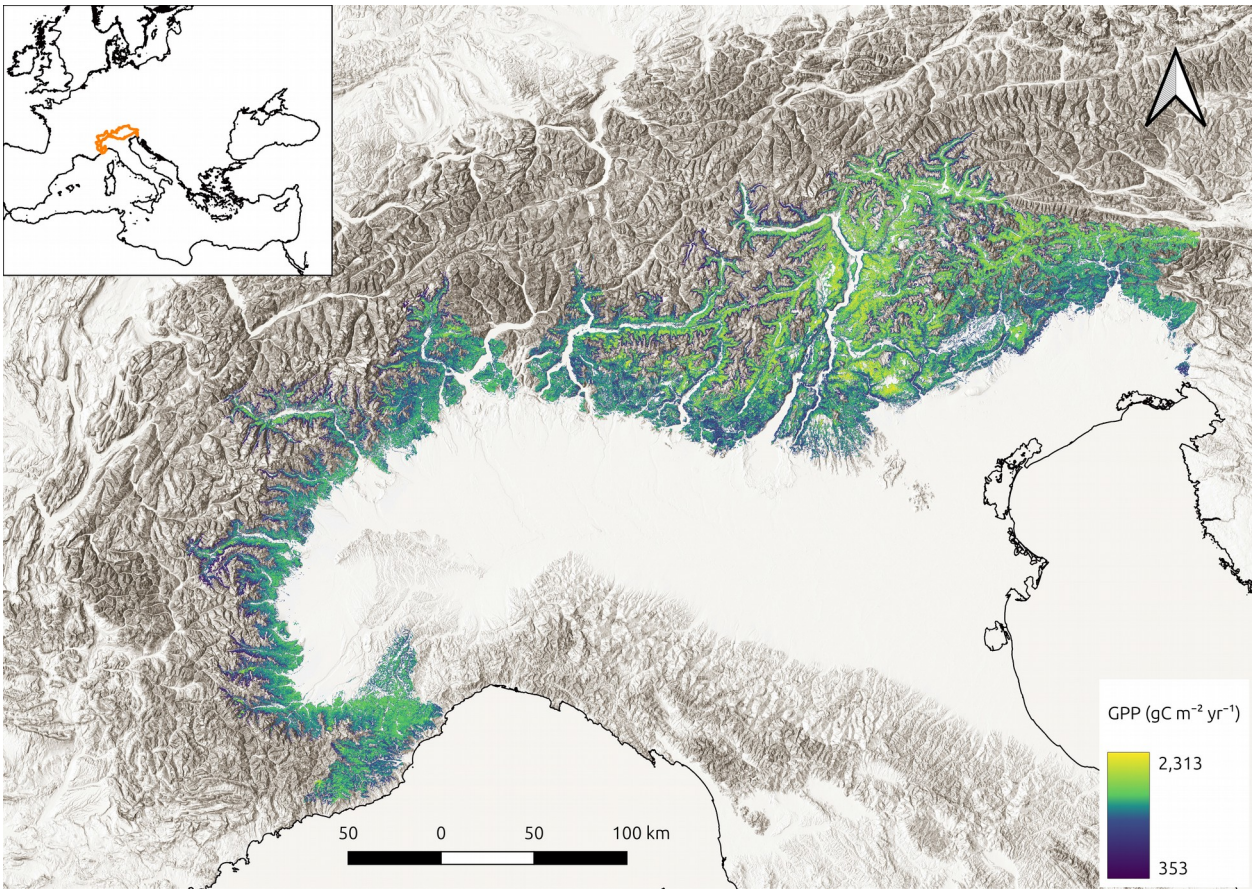


Fig. 2. Wall-to-wall high-resolution (30m) map of GPP (gC m^{-2} yr^{-1}) across the Italian Alps for the test year 2020, generated using a RF algorithm.

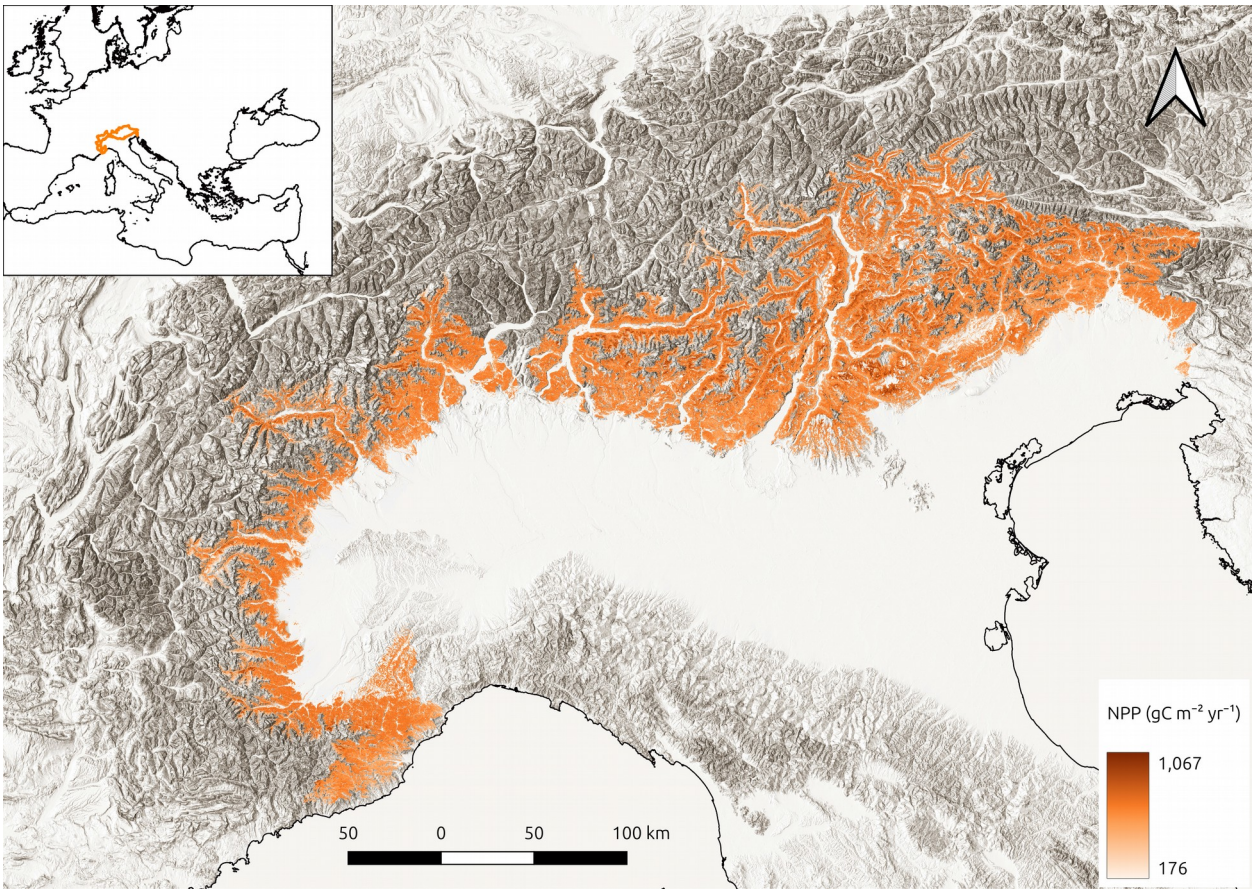


Fig. 3. Wall-to-wall high-resolution (30m) map of NPP (gC m^{-2} yr^{-1}) across the Italian Alps for the test year 2020, generated using a RF algorithm.

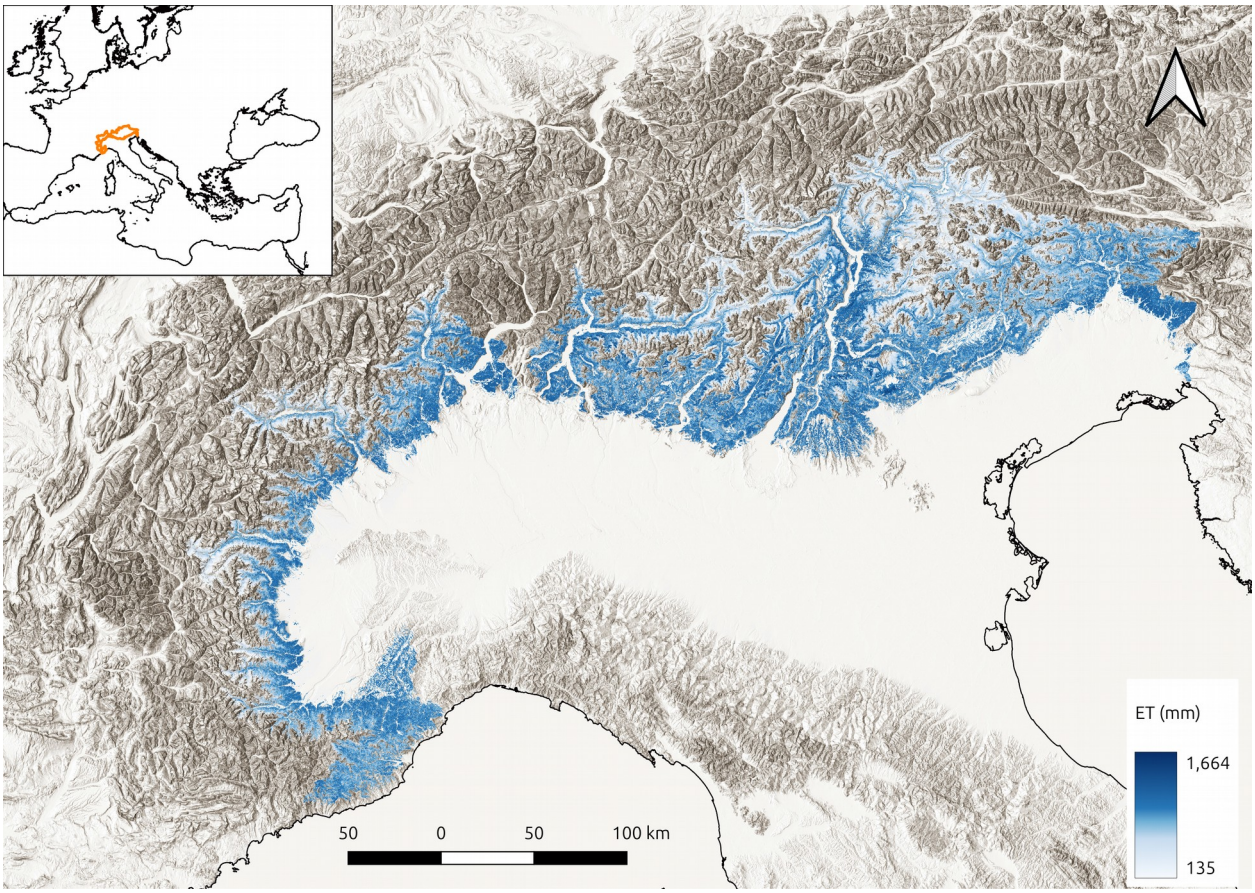


Fig. 4. Wall-to-wall high-resolution map of ET (mm) across the Italian Alps for the test year 2020, generated using a RF algorithm.

Table 2. The coefficient of determination (R^2), the Root Mean Square Error (RMSE) and Percentage Root Mean Square Error (RMSE%) averaged over 5 folds for the GPP (gC m^{-2} yr^{-1}), NPP (gC m^{-2} yr^{-1}) and ET (mm) of the machine learning algorithms performed for the year 2020 over the Italian Alps.

Variables	GPP			NPP			ET		
Metrics	R^2	RMSE	RMSE%	R^2	RMSE	RMSE%	R^2	RMSE	RMSE%
Random Forest (RF)	0.40	394.54	25.61	0.28	177.07	27.02	0.27	480.71	59.13
Extreme Gradient Boosting (XGB)	0.35	411.06	26.65	0.24	182.40	27.82	0.14	524.22	64.36
Artificial Neural	0.31	424.51	27.52	0.18	190.16	28.99	0.19	507.09	62.34

Network (ANN)									
Support Vector Machine (SVM)	0.39	398.03	25.82	0.27	178.93	27.30	0.24	494.78	60.81

458

459 ### 3.2 Feature analysis

460 The RFECV procedure for the GPP, NPP, and ET targets identified optimal subsets of
461 fifteen, thirteen, and nineteen predictors, respectively (Figs. S1-S2-S3). Beyond these
462 thresholds, a decline in test accuracy was observed, suggesting that the inclusion of
463 additional features introduced noise or redundant information. While the specific
464 performance peaks may vary slightly depending on the cross-validation strategy, these
465 subsets represent the optimal balance between model parsimony and predictive power
466 for each flux target. The relative contribution of these predictors was further elucidated
467 through permutation importance analysis (Figs. S4-S5-S6). By quantifying the increase in
468 prediction error following the random shuffling of feature values, we identified the
469 primary environmental and biophysical drivers for each variable. The most influential
470 drivers for GPP included biomass and structural metrics (AGB, CHM), phenological
471 indicators (SOSD, TCW), and moisture-related indices (NDMI), alongside climatic and
472 topographic variables such as Temperature, Wind_ speed, DEM, and Slope. The NPP was
473 predominantly driven by moisture availability (NDMI) and vegetation structure (CHM,
474 AGB, LAI). Additionally, the model utilized thermal and topographic constraints
475 (Temperature, DEM), phenological indicators (TCW, SOSD, EOSV, Length), as well as
476 climatic variables (Precipitation and Wind_speed). ET, in contrast to the productivity
477 targets, was primarily governed by energy and moisture gradients. Temperature, NDMI,
478 and DEM emerged as the top predictors, supplemented by canopy structure (CHM, LAI),
479 atmospheric conditions (Wind_speed, Relative humidity, and Precipitation) and
480 phenological indicators (RSLOPE, SOSD, SPROD and MAXV).

481 ### 3.3 PDP results

The partial dependence plot illustrates the effect of each input variable on GPP, NPP, and ET (Figs. 5-6-7). Biomass (AGB and GSV) exerted a strong positive impact on GPP, increasing from 1350 to 1750 gC m^{-2} yr^{-1} with rising biomass. Similar positive trends occurred with increasing NDMI and CHM. LAI showed a slight increase from 1500 to 1600 gC m^{-2} yr^{-1}, as did temperature (from 1400 to 1600 gC m^{-2} yr^{-1} at higher values). DEM negatively affected GPP at higher altitudes, decreasing from 1600 to 1400 gC m^{-2} yr^{-1}, while eastness yielded a steady slight rise from 1500 to 1600 gC m^{-2} yr^{-1} toward eastern exposures. LSLOPE declined from 1650 to 1450 gC m^{-2} yr^{-1}; precipitation remained stable between 1500 and 1600 gC m^{-2} yr^{-1}; SNOWDPTH decreased from 1600 to 1450 gC m^{-2} yr^{-1} with reduced depth; and SOSD stayed constant near 1600 gC m^{-2} yr^{-1} before dropping to 1400 gC m^{-2} yr^{-1}. Slope caused a decline from 1550 to 1450 gC m^{-2} yr^{-1} with steeper angles; TCW held steady at 1500 gC m^{-2} yr^{-1} before rising to 1600 gC m^{-2} yr^{-1} as TCW decreased; and Wind_speed fluctuated between 1600 and 1500 gC m^{-2} yr^{-1}.

Similar results were obtained for NPP (Fig. 6), with biomass (AGB and GSV) showing a strong positive effect, rising from 600 to 700 gC m^{-2} yr^{-1} as biomass increased. NDMI and CHM exhibited comparable positive trends, with NDMI even more pronounced at higher values. LAI produced a modest gain from 620 to 680 gC m^{-2} yr^{-1}, as similar as Temperature's slight increase that was from 620 to 680 gC m^{-2} yr^{-1} at higher values. DEM reduced NPP at elevated altitudes (from 680 to 600 gC m^{-2} yr^{-1}), while EVI2 drove a slight increase from 640 to 680 gC m^{-2} yr^{-1}. SOSD declined from 680 to 620 gC m^{-2} yr^{-1}; EOSV rose slightly then decreased between 640 and 660 gC m^{-2} yr^{-1}; TCW rose from 640 to 700 gC m^{-2} yr^{-1} at higher values; SNOWDPTH increased from 620 to 680 gC m^{-2} yr^{-1} with greater depth; and SWE showed a slight increase from 620 to 680 gC m^{-2} yr^{-1}.

ET responses differed from those of GPP and NPP. Biomass (GSV) had a marginal effect, ranging from 750 to 850 mm, as shown by the CHM. DEM showed a more pronounced negative impact than for GPP or NPP, with reductions starting at mid-elevations and dropping sharply to 650 mm at the highest altitudes (from 900 mm). NDMI significantly increased ET from 650 to 950 mm, with a similar pattern for Temperature (550 to 950 mm). VPD rose from 700 to 850 mm, as also evidenced for EVI2 (750 to 850 mm). Eastness, Northness, LENGHT, MINV, Precipitation, Slope, SPROD, and SOSD remained stable between 800 and 850 mm. RSLOPE decreased slightly mid-range from 850 to 750 mm; Wind_speed declined slightly from 850 to 800 mm; and SNOWDPTH stayed stable initially before dropping from 850 to 750 mm. LST slightly decreased ET from ~900 to 800 mm (Fig. 7).

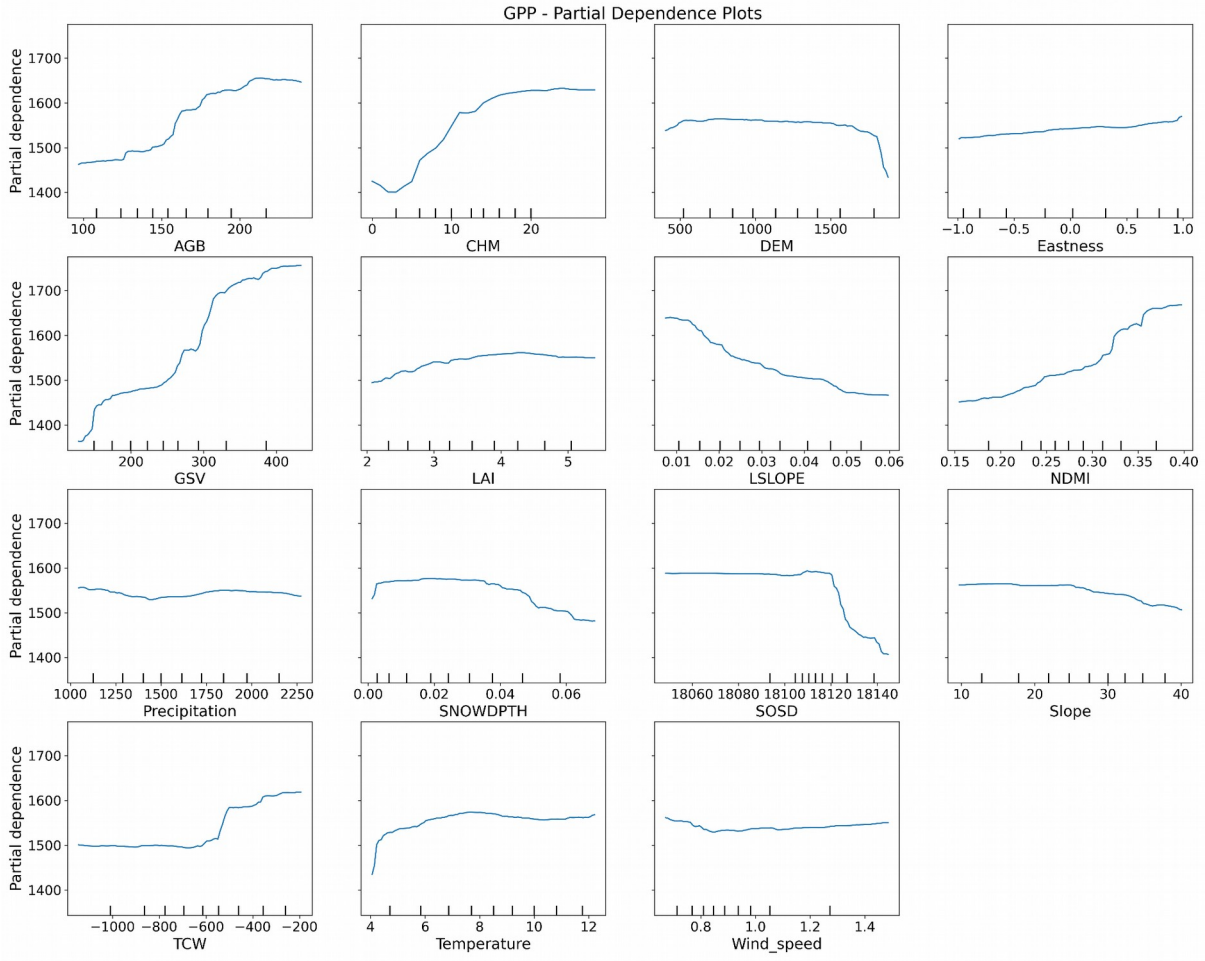


Fig 5. Partial dependence plots for GPP obtained after running the RF algorithm. The above-ground biomass (AGB), canopy height model (CHM), digital elevation model (DEM), aspect (Eastness), growing stock volume (GSV), leaf area index (LAI), slope of the greening phase (LSLOPE), normalized difference moisture index (NDMI), precipitation (Precipitation), snow depth (SNOWDPTH), start of the season-DoY (SOSD), slope (Slope), tasselled cap wetness (TCW), temperature (Temperature), wind speed (Wind_speed).

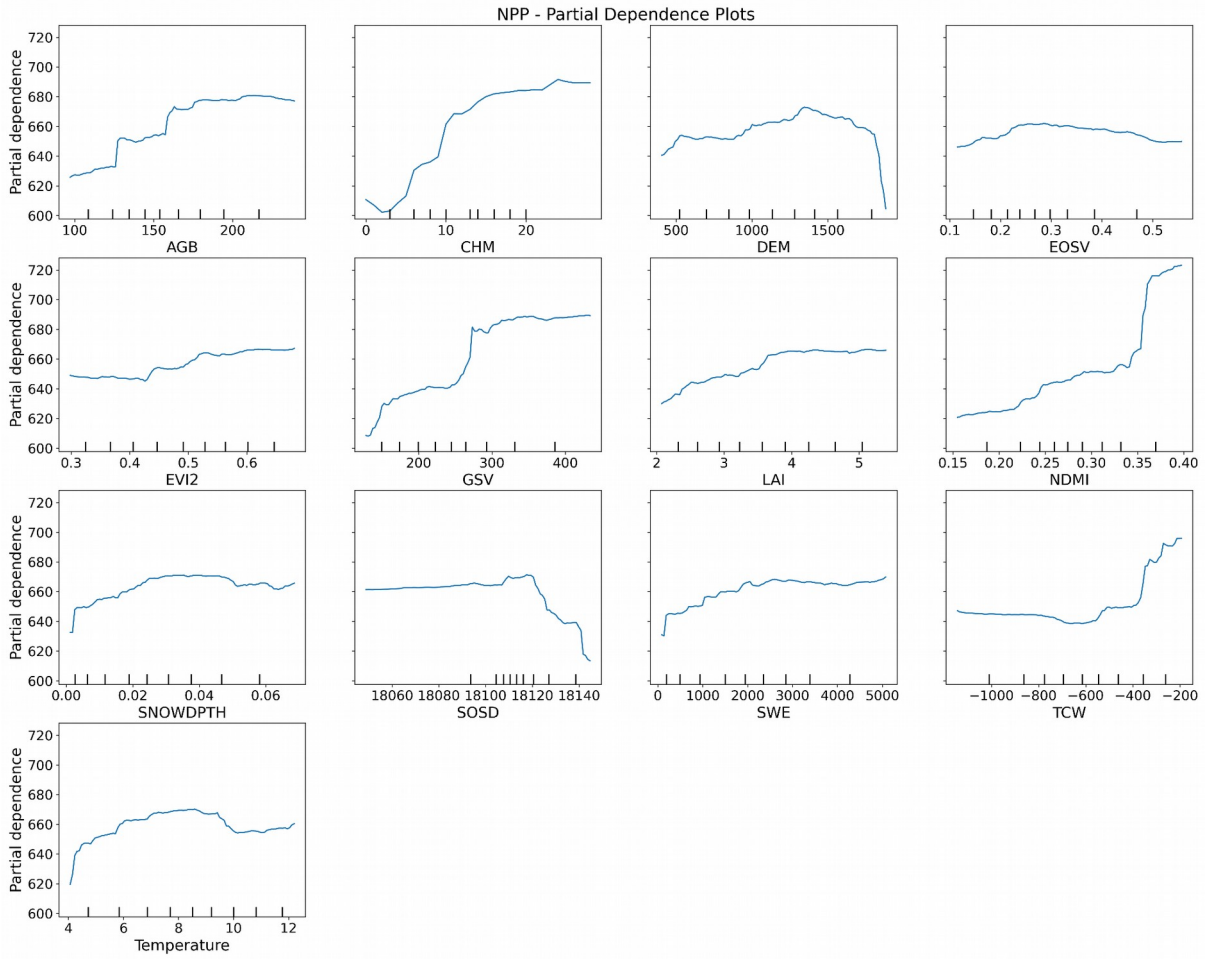


Fig 6. Partial dependence plots for NPP obtained after running the RF algorithm. The above-ground biomass (AGB), canopy height model (CHM), digital elevation model (DEM), end of the season (EOSV), growing stock volume (GSV), leaf area index (LAI), normalized difference moisture index (NDMI), snow depth (SNOWDPTH), start of the season-DoY (SOSD), snow water equivalent (SWE), tasselled cap wetness (TCW), temperature (Temperature).

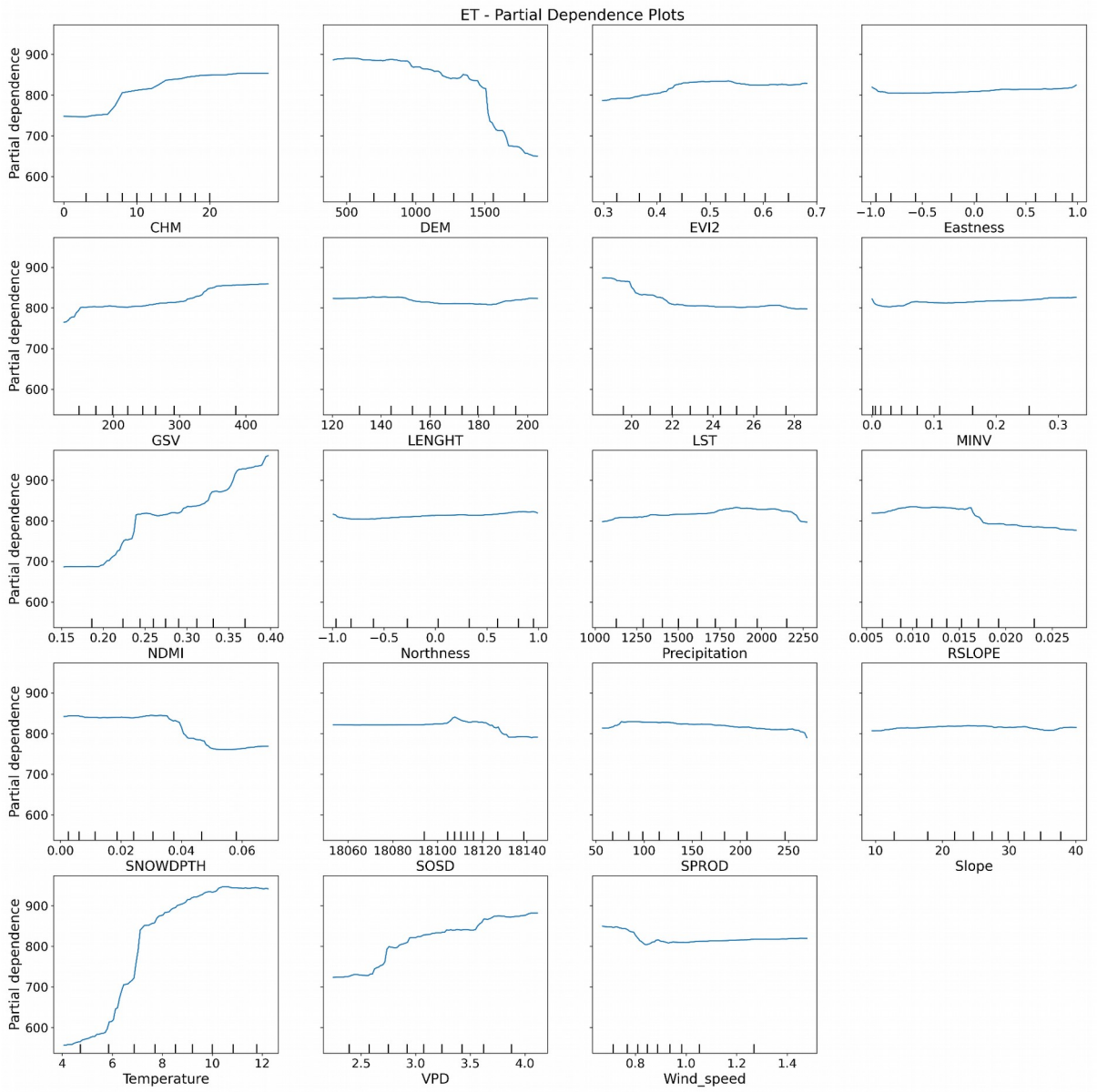


Fig 7. Partial dependence plots for ET obtained after running the RF algorithm. The canopy height model (CHM), digital elevation model (DEM), enhanced vegetation index-2 (EVI2), aspect (Eastness), growing stock volume (GSV), length of the season (LENGHT), land surface temperature (LST), min of the season (MINV), normalized difference moisture index (NDMI), aspect (Northness), precipitation (Precipitation), slope of the browning phase (RSLOPE), snow depth (SNOWDPTH), start of the season-DoY (SOSD), seasonal productivity (SPROD), slope (Slope), temperature (Temperature), vapour pressure deficit (VPD), wind speed (Wind_speed).

3.4 Uncertainty driven by Conformal Prediction

To quantify predictive uncertainty, we wrapped the trained RF regressors in a CP framework (Johansson et al., 2014). This used residual-based nonconformity scores to generate distribution-free prediction intervals with finite-sample coverage guarantees for GPP, NPP, and ET. We added upper and lower bands to the wall-to-wall maps; for GPP, the lower band was 681 gC m^{-2} yr^{-1} and max 2245 gC m^{-2} yr^{-1}; for NPP, the lower band was 264 gC m^{-2} yr^{-1} and the upper band was 997 gC m^{-2} yr^{-1}; and for ET, the lower band was 32 mm and the upper band was 1759 mm.

4 Discussion

With the aim of quantifying the spatial variability of carbon and water fluxes and disentangling their underlying environmental controls, this study integrated process-based model (PBM) simulations, NFI data, RS products, and high-resolution climate information to upscale GPP, NPP, and ET across Italian Alpine forests at a 30 m spatial resolution for 2020. This multi-source framework enabled us not only to generate spatially continuous estimates of these fluxes, but also to assess the relative roles of forest structural, climatic, topographic, and phenological factors in shaping their spatial variability and to quantify the uncertainty associated with the resulting predictions.

Our findings confirm our initial hypotheses regarding the hierarchical control of carbon and water fluxes across Alpine forest ecosystems. In support of H1, forest structural attributes were confirmed as the primary determinants of spatial variability in GPP and NPP. This strong association reveals forest structure as a key constraint on the spatial patterns of carbon assimilation across the complex Alpine landscape, with standing living biomass, stand density, and canopy development jointly shaping GPP and NPP. In addition to forest attributes, canopy and top-soil moisture (represented by NDMI) were a key determinant of both GPP and NPP. In sharp contrast, ET dynamics supported H2, revealing a distinct set of controls on ecosystem water fluxes, which were governed predominantly by atmospheric demand and water availability rather than by forest structural attributes. Climatic and moisture-related variables predominated in explaining ET spatial patterns across the Alpine region, reflecting the overarching influence of VPD, temperature, topography and soil water availability in modulating transpiration and soil evaporation. The relationships observed across the evaluated ML algorithms revealed varying degrees of correlation among estimates derived from different modelling approaches and data sources, with RF showing comparatively stronger correspondence. Rather than indicating the superiority of one approach over another, these differences provide valuable insights into how distinct methodologies capture complementary aspects of ecosystem variability in complex mountainous landscapes. They also highlight opportunities to further improve the integration of these information sources by refining process-based representations of ecosystem dynamics and their parameterization, enhancing the characterization of topographic heterogeneity in RS observations (e.g., spatial resolution and topographic shadowing), and developing ML algorithms capable of better integrating information across steep environmental gradients.By explicitly quantifying the uncertainty associated with our 30 m spatial predictions, this study provides both a robust baseline for regional carbon and water accounting and a transparent evaluation of the performance of the integrated framework.

4.1 Spatial patterns of carbon and water fluxes across the Italian Alps

4.1.1 Carbon fluxes

The spatial distribution of GPP (Fig. 2) reveals the highest values in the northeastern Italian Alps. This is likely attributable to the high prevalence of tall-tree forests, which account for at least 60% of the region's forest cover and higher presence of Norway spruce (well-adapted and highly productive) compared to the western alps (Caudullo et al., 2016; Gasparini & Tabacchi, 2022; Kapeller et al., 2012). Indeed, as emerged from the permutation importance and PDP analyses, the biomass (GSV and AGB) as well as the CHM were the most influential drivers of both gross and net productivity. The highest AGB values, as shown in Fig. S7, are concentrated in the northeastern Alps, consistent with the spatial distribution of GPP. This finding is consistent with Luo et al. (2026), who found that forest structure has an effect on GPP, even if scale-dependent. Nevertheless, numerous other factors can influence carbon fluxes, including forest age, stand density, topography, elevation, exposition and climatic conditions (Brandl et al., 2019; Lewińska et al., 2018; Vangi et al., 2024). A detailed analysis shows that the mean GPP predicted by the RF model (1460 gC m^{-2} yr^{-1}) aligns well with the findings of Fibbi et al. (2019), who reported a GPP range of 1000–1800 gC m^{-2} for the 1981–2090 period. However, a direct comparison is limited because their estimates were derived from a forest model projection. In this regard, Collalti et al. (2016) showed that the 3D-CMCC-FEM model reproduced GPP consistently with eddy covariance observations across diverse forest stands differing in species composition and developmental stage. Consistently, Dalmonech et al. (2024, 2026) further demonstrated the model's ability to reliably simulate GPP at the regional scale, showing good agreement with independent remote sensing and model-based datasets. The more spatially heterogeneous distribution of NPP may be explained by spatial differences in autotrophic respiration (R_a), which are likely associated with the higher biomass observed in the northeastern Alps. Indeed, as trees grow and age, their above- and belowground biomass increases, resulting in greater total volume and, consequently, higher respiratory costs associated with tissue construction and maintenance (West, 2020). Since NPP is calculated as the difference between GPP and R_a (Roxburgh et al., 2005), variation in autotrophic respiration may account for the different spatial patterns observed for the two

productivity metrics. Here, the estimated NPP value (630 gC m^{-2} yr^{-1}) falls within the range reported by Valentini and Miglietta (2014), although referring to a slightly different time period. Similar results were obtained by Trotsiuk et al. (2020) in which the mean value of NPP for the species *Fagus sylvatica* and *Picea abies* was 540 gC m^{-2} yr^{-1} across Switzerland during the 1991–2018 period. A comprehensive comparison across the Alpine region is challenging because datasets available at comparable spatial and temporal resolutions are limited and highly fragmented.

4.1.2 Water fluxes

Concerning ET, as hypothesized, drivers were strongly associated with climatic and moisture-related variables (Fig. 7), with Temperature, NDMI, DEM and VPD emerging as the most influential parameters. The estimated ET value (784 mm yr^{-1}) lies within the upper range reported for vegetated and forested Alpine environments, where annual ET may reach 700–800 mm yr^{-1} at lower elevations, while substantially lower values are reported at high elevations (which can also be seen in Fig.7) due to temperature and energy limitations (Herrnegger et al., 2012). Leng et al. (2024) reported that ET, both measured across an independent dataset of 152 Eddy Covariance towers and simulated by the BEPS model for 2001–2020, ranged from 400 to 800 mm across various global biomes at a 1 km resolution.

ET rates increase with air and soil temperature due to the increased energy driving evaporation from soil and transpiration from plants into the atmosphere (Chaouche et al., 2010; Z. Luo et al., 2026). This process is also regulated by precipitation, which increases soil moisture availability and rises vegetation canopy water content, a shift directly reflected in elevated NDMI values (Gao, 1996; Zhu et al., 2014). Additionally, higher temperatures increase VPD, which acts as the main driver for ET, drawing more water that goes into the atmosphere while simultaneously reducing CO_2 uptake, regardless of soil moisture levels (Sulman et al., 2016).

4.2 Contrasting controls on carbon productivity and evapotranspiration

4.2.1 Carbon fluxes

642 The rational use of PDPs allowed us to draw detailed conclusions regarding the
643 relationships between predictors and target variables, revealing predominantly non-
644 linear responses characterized by threshold effects and saturation patterns. As before
645 mentioned, for GPP and NPP, forest structural attributes such as GSV, CHM, and AGB
646 show strong positive relationships, indicating that more structurally developed and
647 biomass-rich forest stands generally sustain higher photosynthetic activity (Fischer et al.,
648 2019; J. Zhang et al., 2016). However, these relationships tended to plateau at higher
649 values, suggesting diminishing marginal gains in productivity likely associated with
650 canopy competition, increased self-shading and the reduction of the resource use
651 efficiency (Binkley, 2004; Ryan et al., 1997). The observed plateau in GPP and NPP may
652 reflect not only changes in the amount and distribution of standing biomass as forests
653 develop and age (Collalti et al., 2020), but also increasing physiological constraints,
654 particularly hydraulic limitation and a reduced capacity for stomatal regulation (Ryan et
655 al., 2006). Together, these structural and hydraulic constraints can progressively limit
656 stomatal conductance and photosynthetic carbon uptake, ultimately constraining further
657 increases in ecosystem productivity (Ryan & Yoder, 1997; Urban & Urban, 2024).
658 Similarly, LAI (and EVI2 for NPP) exhibited a moderate positive effect, consistent with
659 their well-known rapid saturation at higher vegetation densities, while still supporting
660 the role of leaf area in enhancing carbon assimilation (Cao et al., 2025; Zhao et al.,
661 2021).

Hydrological and vegetation moisture-related predictors also exerted an important influence on GPP and NPP. In particular, productivity increased sharply as NDMI and TCW (and SWE just for NPP) rose past intermediate moisture levels, underscoring how increasing vegetation water status reduces stomatal limitations and promotes photosynthesis. Conversely, for GPP, precipitation exhibited only a marginal effect, suggesting that direct climatic inputs may be less informative than remotely sensed proxies of actual vegetation water content, which more effectively capture plant physiological responses to moisture availability (Flexas & Medrano, 2002; Yan et al., 2016). SNOWDPTH exhibited contrasting relationships with GPP and NPP, with higher snow depth generally associated with reduced GPP, whereas NPP showed a moderate increase under intermediate snow conditions followed by steadying. These differing responses suggest a complex role of snow cover in forest carbon dynamics, well captured by the 3D-CMCC-FEM model, potentially reflecting both the legacy effects of winter snow accumulation on active-season soil moisture and the extent to which vegetation productivity is constrained by water availability (X. Wang et al., 2018; Y. Wang et al., 2024). Temperature, both for GPP and NPP, showed a positive relationship characterized by an initial increase followed by saturation at intermediate values, consistent with the existence of a thermal optimum for photosynthesis, with different response based on environment and species, beyond which gains in carbon assimilation become limited (Medlyn et al., 2002; Yamori et al., 2014). Potential carbon sequestration may be reduced by extreme temperatures, particularly during summer, when drought can limit carbon uptake (e.g. as observed in 2018 and 2022) or even cause ecosystems to become net carbon sources (van der Woude et al., 2023). Wind speed showed a weak and marginal relationship with GPP. SOSD displayed a negative relationship with gross and net productivity, particularly beyond a threshold, indicating that delayed onset of the growing season may substantially constrain annual carbon uptake by shortening the effective photosynthetically active period. This finding reinforces the ecological importance of growing season timing as a determinant of ecosystem productivity (Piao et al., 2007; Pulliainen et al., 2017; Richardson et al., 2009). DEM showed a slight

declining trend at higher elevations, potentially reflecting colder temperatures, shorter growing seasons, and harsher environmental conditions at higher altitudes. Eastness and Slope predictors exhibited relatively minor effects, although the negative response suggests that steeper or morphologically constrained terrain may reduce productivity through lower soil development, reduced water retention capacity, or increased erosional processes (T. Liang et al., 2024; Mehmood et al., 2024; Sun et al., 2025).

4.2.2 Water fluxes

For ET, PDPs revealed response patterns partially consistent with those observed for GPP and NPP, while emphasizing a comparatively stronger influence of climatic controls over forest structural attributes. Although forest structural variables such as CHM and GSV maintained positive relationships with ET, similarly to productivity metrics, their effects were weaker and saturated earlier, suggesting that forest structure contributes to evapotranspirative fluxes but plays a secondary role relative to atmospheric and climatic drivers (see Fig. 7).

ET increased sharply above lower temperature thresholds before gradually approaching saturation, suggesting that warmer conditions strongly enhance evaporative demand and water fluxes until environmental and/or physiological constraints begin to limit further increases (Yang et al., 2023). Similarly, VPD exhibited a positive response, with ET increasing progressively under higher atmospheric water demand. This pattern suggests that increases in atmospheric dryness may enhance water fluxes between vegetation and the atmosphere, although the flattening of the response at higher VPD values (together with the weak negative trend observed for LST) may indicate the onset of physiological regulation, such as partial stomatal closure under excessive evaporative stress (Grossiord et al., 2020; Wen et al., 2024). NDMI exhibited a strong positive relationship with ET, while EVI2 showed a weaker but positive effect, highlighting the importance of vegetation water status and canopy development in sustaining evapotranspirative fluxes (J. Chen et al., 2026; Poon & Kinoshita, 2018). Although evaporation contributes less to ecosystem water fluxes than transpiration, it remains an important component and is strongly influenced by both soil moisture (SM) and VPD (Kozii et al., 2020; Wetzel & Chang, 1987). While rising VPD tends to enhance evaporation, the negative effect of declining SM is expected to dominate, causing evaporation to continue decreasing. This would be even exacerbated in future (H. Chen & Wei, 2025).

DEM showed a marked negative relationship with ET, particularly at higher elevations, where ET declined substantially. This pattern may reflect cooler conditions, reduced atmospheric energy availability, and lower evaporation demand at higher altitudes as well as the species composition (Goulden & Bales, 2014; Hu et al., 2023). Eastness, Northness and Slope exhibited relatively weak effects, indicating that local terrain configuration exerted only a limited control on ET variability. Likewise, HRVPP-derived variables (MINV, LENGHT, SOSD, SPROD, and RSLOPE) showed weak and largely stable responses, highlighting a comparatively minor role of phenological dynamics relative to climatic and hydrological drivers. SNOWDPTH showed a negative relationship, with ET declining under higher snow depth conditions. This suggests reduced annual water fluxes in environments characterized by greater snow persistence, which delays the onset of spring snowmelt and limits the early-season growing window (Molotch et al., 2009). Among the remaining climatic variables, Wind_speed exhibited a weak and non-linear response as also evidenced in Zhang et al. (2025), characterized by an initial decline followed by a relatively constant trend. Precipitation showed only a modest effect, with ET remaining relatively stable and slightly declining at higher values, suggesting limited additional contributions of precipitation to ET fluxes in the Alpine regions where water is not a limiting factor so far (Ménégoz et al., 2020).

4.3 Predictive performance and uncertainty of the integrated framework

743 RF showed the highest predictive accuracy for GPP, NPP, and ET, followed by SVM, XGB,
744 and ANN, consistent with previous findings (Tian et al., 2024; Xu et al., 2018). A possible
745 explanation is that ecological variables often exhibit nonlinear and interacting effects on
746 response variables, and RF is particularly well suited to account for these complexities
747 without imposing parametric assumptions on predictor–response relationships
748 (Breiman, 2001; Olden et al., 2008). The correlations obtained with RF (R^2 = 0.40, 0.28,
749 and 0.27 for GPP, NPP, and ET, respectively) provide insights into the degree of
750 correspondence between different sources of information, reflecting the ecological
751 complexity and spatial heterogeneity of Alpine forest ecosystems, as well as the
752 stringent validation framework adopted in this study.We used a spatial block cross-
753 validation strategy to explicitly evaluate model transferability across geographically
754 independent forest stands (Roberts et al., 2017). However, in our case, the discrepancy
755 between spatial and conventional cross-validation was negligible, suggesting that spatial
756 autocorrelation did not substantially inflate predictive performance. Therefore, the
757 moderate predictive accuracy likely reflects the strong environmental heterogeneity of
758 Alpine forests, local ecological variability, and ecological processes not fully captured by
759 the available predictors. Similar limitations have been reported previously in spatial
760 ecological prediction and forest productivity modeling, where transferability across
761 heterogeneous landscapes remains inherently challenging (Gaber et al., 2024; Ploton et
762 al., 2020). Despite the overall consistency of the predicted mean values with previous
763 findings, both GPP and NPP showed limited model performance in reproducing the tails
764 of the distribution (see Fig. S8 and S9 in Supplementary Material). In particular, the RF
765 model tended to smooth extreme values, resulting in a weaker agreement between
766 observed and predicted values at the lower and upper ends of the range. This behaviour
767 suggests that the RF captured the central tendency of carbon flux dynamics reasonably
768 well, while struggling to represent extreme productivity conditions. Similar limitations
769 have also been reported by Zhang et al. (2020) in forest ecosystem studies, where RF
770 models tend to underestimate high values and overestimate low values, leading to
771 reduced accuracy at the tails of the distribution. This pattern remained evident despite

772 extensive hyperparameter tuning and exploratory tests aimed at improving model
773 sensitivity to extreme values through data augmentation approaches targeting tail
774 observations (here not shown), suggesting that the limited representation of extreme
775 productivity conditions may partly reflect an intrinsic limitation of the RF regression
776 framework. A similar behaviour was observed for ET, although in this case the reduced
777 predictive performance was mainly restricted to the upper tail of the distribution, where
778 high ET values tended to be underestimated (Fig. S10). In addition, the observed
779 underestimation of high ET values may partly arise from processes not explicitly
780 represented in the model, such as nighttime ET, which can contribute to total ET under
781 specific environmental conditions (de Jong, 2025).

Although the 3D-CMCC-FEM model has repeatedly demonstrated its ability to simulate carbon and water fluxes across boreal, temperate, and Mediterranean forests (see also (Mahnken et al., 2022), further improvements are still needed. Moreover, it is important to highlight that a general, not point-level and literature-based, species-specific parameterization was used, without calibration for the species occurring in the Alpine region. In addition, the simulations were performed for the entire Italian national territory rather than exclusively for the Alpine region. Another source of uncertainty affecting carbon and water fluxes estimates may arise from the contribution of the understory, which was not included in the model simulations and not captured in the predictors, as also evidenced in the results of the study of Dirnböck et al. (2020). The major sources of uncertainty likely arise from the limited number of predictors included, as well as the aggregations/averaging of highly dynamic predictors over a whole year, which may not fully capture the complexity required to accurately estimate carbon and water fluxes in a highly heterogeneous environment such as the Alpine ecosystem. For example, nitrogen deposition (when not excessive) may enhance both carbon sequestration and transpiration (X. Liang et al., 2020; Wortman et al., 2012), while elevated atmospheric CO_2 concentrations may further stimulate carbon sequestration (de Wergifosse et al., 2022). Finally, an additional source of uncertainty may stem from disturbance factors that were neither included as predictors nor simulated by the 3D-CMCC-FEM model. These include pest outbreaks (e.g., bark beetles and other biotic agents), climatic extremes such as late frost, windstorm, drought events, and human activities which may substantially affect forest carbon and water fluxes (Boukhris et al., 2026; L. Chen et al., 2023; Coops & Wulder, 2010; Motta et al., 2018; J. Wang et al., 2025).

6 Conclusions

Estimating GPP, NPP, and ET fluxes in forest ecosystems, particularly in Alpine forests, remains a major challenge due to the complexity of ecological processes and the high heterogeneity of mountain environments, where topography and environmental conditions vary substantially over short spatial scales. Nevertheless, the integration of complementary approaches such as process-based forest modeling, remote sensing, and machine learning can substantially improve our ability to characterize ecosystem dynamics. In this study, the combination of these inherently different approaches enabled the estimation of GPP, NPP, and ET across the entire Italian Alpine region, producing high-resolution (30m) wall-to-wall maps. Among the four machine learning algorithms tested, Random Forest showed the best performance and proved to be an effective approach for spatializing ecosystem fluxes across such a heterogeneous environment. Although further improvements may be achieved through enhanced representation of ecological processes in forest models, higher spatial and temporal resolution remote sensing products, and continued advances in machine learning methodologies, the results of this study demonstrate the strong potential of integrated frameworks to provide spatially explicit information on forest carbon and water dynamics. The resulting 30 m resolution wall-to-wall maps provide an unprecedented level of detail on GPP, NPP, and ET dynamics across Italian Alpine forests for the year 2020. These products can support ecosystem monitoring, improve carbon budget assessments, and inform future forest management strategies under changing environmental conditions, ultimately contributing to climate change adaptation and mitigation efforts.

Author contributions:

Vincenzo Saponaro: Conceptualization, Methodology, Data curation, Formal analysis, Software development, Writing – original draft, Writing – review & editing. **Elia Vangi:** Conceptualization, Methodology, Data curation, Formal analysis, Software development, Writing – original draft, Writing – review & editing. **Anna Candotti:** Conceptualization, Data curation, Writing – review & editing. **Daniela Dalmonech:** Writing – review & editing. **Marta Galvagno:** Writing – review &

editing. **Gianluca Filippa:** Writing – review & editing. **Alessio Collalti:** Writing – review & editing. **Enrico Tomelleri:** Conceptualization, Methodology, Supervision, project Administration, Writing – review & editing.

Open Research section

In accordance with AGU policy on the use of AI tools, the authors acknowledge the use of Anthropic's Claude and Google's Gemini in the preparation of this work. These AI tools were used for grammatical editing, sentence rewording, and code debugging. All AI-assisted text and code were thoroughly reviewed, tested, and verified by the authors, who take full responsibility for the content of the manuscript.

Acknowledgments

V.S. was founded by iNEST (Interconnected North-East Innovation Ecosystem) the European UnionNext GenerationEU – PNRR (Italian National Plan for Recovery and Resilience) Missione 4 Componente 2, Investimento 1.5 D.D. 1058 23/06/2022, ECS_00000043 –Spoke1, CUP I43C22000250006). This manuscript reflects only the Authors views and opinions, neither the European Union nor the European Commission can be considered responsible for them. E.V. acknowledge the H2020 NextGenCarbon project funded by the European Commission, number 101184989 call HORIZON-CL5-2024-D1-01-07. AC was supported by the Cohesion Italy 21-27 Project EFRE1079 "Forest Robotic Monitoring and Automation (FORMA)", co-funded by the EU and the Autonomous Province of Bozen-Bolzano.

Data Availability Statement:

The codes and predictors data used for creating high-resolution maps in this study, as well as the maps created, are available at Zenodo repository via 10.5281/zenodo.23065081 with Creative Commons Attribution 4.0 International (CC BY 4.0). Additional predictor variables were obtained from public repositories. Specifically, DEM data were retrieved from TINITALY (https://tinitaly.pi.ingv.it/); EVI2 and NDMI from Copernicus Sentinel-2 Surface Reflectance via Google Earth Engine (https://developers.google.com/earth-engine/datasets/catalog/COPERNICUS_S2_SR_HARMONIZED); FTY from Copernicus High Resolution Layers (https://land.copernicus.eu/en/products/high-resolution-layer-forests-and-tree-cover); LST from Landsat 8 via Google Earth Engine (https://developers.google.com/earth-engine/datasets/catalog/LANDSAT_LC08_C02_T1_L2); CHM from the GEE Community Catalog (https://gee-community-catalog.org/projects/meta_trees/); species distributions from Zenodo (https://zenodo.org/records/13341104); HRVPP from Copernicus (https://land.copernicus.eu/en/news/high-resolution-phenology-and-productivity-annual-product-update); and LAI from Copernicus Vegetation (https://land.copernicus.eu/en/products/vegetation/leaf-area-index-300m-v1.0).

Conflict of Interest Disclosure

The authors declare that they have no known competing financial interests or personal relationships that could have influenced the work reported in this paper.

References

Alsafadi, K., Bashir, B., Mohammed, S., Abdo, H. G., Mokhtar, A., Alsalman, A., & Cao, W. (2024). Response of ecosystem carbon–water fluxes to extreme drought in west Asia. *Remote Sensing*, *16*(7), 1179. https://doi.org/10.3390/rs16071179

Altmann, A., Toloşi, L., Sander, O., & Lengauer, T. (2010). Permutation importance: a corrected feature importance measure. *Bioinformatics (Oxford, England)*, *26*(10), 1340–1347. https://doi.org/10.1093/bioinformatics/btq134

Amthor, J. (2000). The McCree–de Wit–penning de Vries–Thornley respiration paradigms: 30 years later. *Annals of Botany*, *86*(1), 1–20. https://doi.org/10.1006/anbo.2000.1175

Angelopoulos, A. N., & Bates, S. (2021). A gentle introduction to conformal prediction and distribution-free uncertainty quantification. In *arXiv [cs.LG]*. arXiv. https://doi.org/10.48550/arXiv.2107.07511

Araza, A., de Bruin, S., Hein, L., & Herold, M. (2023). Spatial predictions and uncertainties of forest carbon fluxes for carbon accounting. *Scientific Reports*, *13*(1), 12704. https://doi.org/10.1038/s41598-023-38935-8

Avanzi, F., Munerol, F., Milelli, M., Gabellani, S., Massari, C., Girotto, M., Cremonese, E., Galvagno, M., Bruno, G., Morra di Cella, U., Rossi, L., Altamura, M., & Ferraris, L. (2024). Winter snow deficit was a harbinger of summer 2022 socio-hydrologic drought in the Po Basin, Italy. *Communications Earth & Environment*, *5*(1). https://doi.org/10.1038/s43247-024-01222-z

Barzani, A. R., Pahlavani, P., Ghorbanzadeh, O., Gholamnia, K., & Ghamisi, P. (2024). Evaluating the impact of recursive feature elimination on machine learning models for predicting forest fire-prone zones. *Fire*, *7*(12), 440. https://doi.org/10.3390/fire7120440

Binkley, D. (2004). A hypothesis about the interaction of tree dominance and stand production through stand development. *Forest Ecology and Management*, *190*(2-3), 265–271. https://doi.org/10.1016/j.foreco.2003.10.018

Bonan, G. B. (2008). Forests and climate change: forcings, feedbacks, and the climate benefits of forests. *Science (New York, N.Y.)*, *320*(5882), 1444–1449. https://doi.org/10.1126/science.1155121

Bonan, G. B., Williams, M., Fisher, R. A., & Oleson, K. W. (2014). Modeling stomatal conductance in the earth system: linking leaf water-use efficiency and water transport along the soil–plant–atmosphere continuum. *Geoscientific Model Development*, *7*(5), 2193–2222. https://doi.org/10.5194/gmd-7-2193-2014

Boukhris, I., Cherubini, F., Collalti, A., Dalmonech, D., Vonderach, C., Marano, G., Giannetti, F., Lahssini, S., Santini, M., & Valentini, R. (2026). Long-term forest-sector mitigation and radiative forcing under contrasting management, climate, and substitution pathways. *Journal of Environmental Management*, *405*(129586), 129586. https://doi.org/10.1016/j.jenvman.2026.129586

Boukhris, I., Marano, G., Dalmonech, D., Valentini, R., & Collalti, A. (2025). Modeling forest growth under current and future climate. *Current Forestry Reports*, *11*(1). https://doi.org/10.1007/s40725-025-00249-5

Brandl, S., Falk, W., Rötzer, T., & Pretzsch, H. (2019). Assessing site productivity based on national forest inventory data and its dependence on site conditions for spruce dominated forests in Germany. *Forest Systems*, *28*(2), e007. https://doi.org/10.5424/fs/2019282-14423

Breiman, L. (2001). Random forests. *Machine Learning*, *45*(1), 5–32. https://doi.org/10.1023/a:1010933404324

924Brighenti, S., Obojes, N., Bertoldi, G., Zuecco, G., Censini, M., Cassiani, G., Penna, D., &
925 Comiti, F. (2024). Snowmelt and subsurface heterogeneity control tree water sources in a
926 subalpine forest. *Ecohydrology: Ecosystems, Land and Water Process Interactions, Ecohydrogeomorphology*, *17*(7). https://doi.org/10.1002/eco.2695
928Brown, C. F., Kazmierski, M. R., Pasquarella, V. J., Rucklidge, W. J., Samsikova, M., Zhang,
929 C., Shelhamer, E., Lahera, E., Wiles, O., Ilyushchenko, S., Gorelick, N., Zhang, L. L., Alj,
930 S., Schechter, E., Askay, S., Guinan, O., Moore, R., Boukouvalas, A., & Kohli, P. (2025).
931 AlphaEarth Foundations: An embedding field model for accurate and efficient global
932 mapping from sparse label data [Dataset]. In *arXiv [cs.CV]*. arXiv. https://doi.org/10.48550/
933 arXiv.2507.22291
934Brunetti, M., Lentini, G., Maugeri, M., Nanni, T., Auer, I., Böhm, R., & Schöner, W. (2009).
935 Climate variability and change in the Greater Alpine Region over the last two centuries
936 based on multi-variable analysis. *International Journal of Climatology: A Journal of the*
937 *Royal Meteorological Society*, *29*(15), 2197–2225. https://doi.org/10.1002/joc.1857
938Brunetti, M., Maugeri, M., Monti, F., & Nanni, T. (2006). Temperature and precipitation
939 variability in Italy in the last two centuries from homogenised instrumental time series.
940 *International Journal of Climatology: A Journal of the Royal Meteorological Society*, *26*(3),
941 345–381. https://doi.org/10.1002/joc.1251
942C3S. (2018). *ERA5 hourly data on single levels from 1940 to present* [Dataset]. Copernicus
943 Climate Change Service (C3S) Climate Data Store (CDS).
944 https://doi.org/10.24381/CDS.ADBB2D47
945Candotti, A., & Tomelleri, E. (2026). High-resolution above-ground biomass mapping of the
946 Alps using satellite embeddings and GEDI. In Earth System Science Data Discussions.

947 Earth System Science Data Discussions. https://doi.org/10.5194/essd-2026-798

948Cao, D., Huang, X., Liu, G., Tian, L., Xin, Q., & Yang, Y. (2025). Evaluating the performance
949 of satellite-derived vegetation indices in gross primary productivity (GPP) estimation at 30
950 m and 500 m spatial resolution. *Remote Sensing*, *17*(19), 3291.
951 https://doi.org/10.3390/rs17193291

952Caudullo, G., Tinner, W., & de Rigo, D. (2016). *Picea abies in Europe: distribution, habitat,*
953 *usage and threats*. University of Bern. https://doi.org/10.7892/BORIS.80794

954Chaouche, K., Neppel, L., Dieulin, C., Pujol, N., Ladouche, B., Martin, E., Salas, D., &
955 Caballero, Y. (2010). Analyses of precipitation, temperature and evapotranspiration in a
956 French Mediterranean region in the context of climate change. *Comptes Rendus:*
957 *Geoscience*, *342*(3), 234–243. https://doi.org/10.1016/j.crte.2010.02.001

958Chen, H., & Wei, Y. (2025). Declining soil evaporation on a drying earth. *Agricultural and*
959 *Forest Meteorology*, *368*(110550), Not Available.
960 https://doi.org/10.1016/j.agrformet.2025.110550

961Chen, J., Stoy, P. C., & Zhang, Z. (2026). Improved joint estimation of daily actual
962 evapotranspiration and gross primary production by integrating Landsat, Sentinel-2,
963 Sentinel-1, and climate data with machine learning. *Journal of Geophysical Research.*
964 *Biogeosciences*, *131*(4). https://doi.org/10.1029/2025jg009246

965Chen, L., Keski-Saari, S., Kontunen-Soppela, S., Zhu, X., Zhou, X., Hänninen, H., Pumpanen, J.,
966 Mola-Yudego, B., Wu, D., & Berninger, F. (2023). Immediate and carry-over effects of
967 late-spring frost and growing season drought on forest gross primary productivity capacity
968 in the Northern Hemisphere. *Global Change Biology*, *29*(14), 3924–3940.
969 https://doi.org/10.1111/gcb.16751

Chen, T., & Guestrin, C. (2016). XGBoost: A Scalable Tree Boosting System. *Proceedings of the 22nd ACM SIGKDD International Conference on Knowledge Discovery and Data Mining*, 785–794. https://doi.org/10.1145/2939672.2939785

Collalti, A., Dalmonech, D., Vangi, E., Marano, G., Puchi, P. F., Morichetti, M., Saponaro, V., Orrico, M. R., & Grieco, E. (2024). *Monitoring and Predicting Forest Growth and Dynamics*. CNR Edizioni. https://doi.org/10.32018/ForModLab-book-2024

Collalti, A., Ibrom, A., Stockmarr, A., Cescatti, A., Alkama, R., Fernández-Martínez, M., Matteucci, G., Sitch, S., Friedlingstein, P., Ciais, P., Goll, D. S., Nabel, J. E. M. S., Pongratz, J., Arneth, A., Haverd, V., & Prentice, I. C. (2020). Forest production efficiency increases with growth temperature. *Nature Communications*, *11*(1), 5322. https://doi.org/10.1038/s41467-020-19187-w

Collalti, A., Marconi, S., Ibrom, A., Trotta, C., Anav, A., D'Andrea, E., Matteucci, G., Montagnani, L., Gielen, B., Mammarella, I., Grünwald, T., Knohl, A., Berninger, F., Zhao, Y., Valentini, R., & Santini, M. (2016). Validation of 3D-CMCC Forest Ecosystem Model (v.5.1) against eddy covariance data for 10 European forest sites. *Geoscientific Model Development*, *9*(2), 479–504. https://doi.org/10.5194/gmd-9-479-2016

Collalti, A., Perugini, L., Santini, M., Chiti, T., Nolè, A., Matteucci, G., & Valentini, R. (2014). A process-based model to simulate growth in forests with complex structure: Evaluation and use of 3D-CMCC Forest Ecosystem Model in a deciduous forest in Central Italy. *Ecological Modelling*, *272*, 362–378. https://doi.org/10.1016/j.ecolmodel.2013.09.016

Coops, N. C., & Wulder, M. A. (2010). Estimating the reduction in gross primary production due to mountain pine beetle infestation using satellite observations. *International Journal of Remote Sensing*, *31*(8), 2129–2138. https://doi.org/10.1080/01431160903474947

COP26. (2021). *COP26: The Glasgow Climate Pact*. https://ukcop26.org/wp-content/uploads/2021/11/COP26-Presidency-Outcomes-The-Climate-Pact.pdf

Copernicus Land Monitoring Service, & Copernicus Land Monitoring Service Helpdesk. (2017). Leaf Area Index 2014-present (raster 300 m), global, 10-daily - version 1 [Dataset]. Copernicus Land Monitoring Service. https://doi.org/10.2909/219FDC9F-616B-444B-A495-198F527B4722

Cortes, C., & Vapnik, V. (1995). Support-vector networks. *Machine Learning*, *20*(3), 273–297. https://doi.org/10.1007/bf00994018

Dalmonech, D., Vangi, E., Chiesi, M., Chirici, G., Fibbi, L., Giannetti, F., Marano, G., Massari, C., Nolè, A., Xiao, J., & Collalti, A. (2024). Regional estimates of gross primary production applying the Process-Based Model 3D-CMCC-FEM vs. Remote-Sensing multiple datasets. *European Journal of Remote Sensing*, *57*(1). https://doi.org/10.1080/22797254.2023.2301657

Dalmonech, D., Vangi, E., Quesada Chacón, D., & Collalti, A. (2026). Decadal climate-driven decoupling between gross primary productivity and tree growth in Mediterranean forests. *Forest Ecology and Management*, *615*(123843), 123843. https://doi.org/10.1016/j.foreco.2026.123843

Danesh, T., Ouaret, R., & Floquet, P. (2022). *Interpretability in machine learning predictions: case of Random Forest regression using Partial Dependence Plots*. hal.science. https://hal.science/hal-03841177/document

de Jong, C. (2025). A review of experimental evapotranspiration in mountain environments. In *Evapotranspiration in Agro-Ecosystems and Forestry* (pp. 187–220). Elsevier.

https://doi.org/10.1016/b978-0-443-21649-7.00005-5

De Keersmaecker, W., Zanaga, D., Senf, C., Viana-Soto, A., Klapper, J., Blickensdörfer, L., Govaere, L., Lerink, B., Leyman, A., Schelhaas, M.-J., Teeuwen, S., Verkerk, P. J., & Van De Kerchove, R. (2024). ForestPaths: European tree genus map [Dataset]. Zenodo. https://doi.org/10.5281/ZENODO.13341104

de Pury, D. G. G., & Farquhar, G. D. (1997). Simple scaling of photosynthesis from leaves to canopies without the errors of big-leaf models. *Plant, Cell & Environment*, *20*(5), 537–557. https://doi.org/10.1111/j.1365-3040.1997.00094.x

de Wergifosse, L., André, F., Goosse, H., Boczon, A., Cecchini, S., Ciceu, A., Collalti, A., Cools, N., D'Andrea, E., De Vos, B., Hamdi, R., Ingerslev, M., Knudsen, M. A., Kowalska, A., Leca, S., Matteucci, G., Nord-Larsen, T., Sanders, T. G., Schmitz, A., … Jonard, M. (2022). Simulating tree growth response to climate change in structurally diverse oak and beech forests. *The Science of the Total Environment*, *806*(Pt 2), 150422. https://doi.org/10.1016/j.scitotenv.2021.150422

Dirnböck, T., Kraus, D., Grote, R., Klatt, S., Kobler, J., Schindlbacher, A., Seidl, R., Thom, D., & Kiese, R. (2020). Substantial understory contribution to the C sink of a European temperate mountain forest landscape. *Landscape Ecology*, *35*(2), 483–499. https://doi.org/10.1007/s10980-019-00960-2

Dixon, B., & Candade, N. (2008). Multispectral landuse classification using neural networks and support vector machines: one or the other, or both? *International Journal of Remote Sensing*, *29*(4), 1185–1206. https://doi.org/10.1080/01431160701294661

Dou, X., Yang, Y., & Luo, J. (2018). Estimating forest carbon fluxes using machine learning techniques based on eddy covariance measurements. *Sustainability*, *10*(1), 203.

https://doi.org/10.3390/su10010203

Dubayah, R. O., Armston, J., Kellner, J. R., Duncanson, L., Healey, S. P., Patterson, P. L., Hancock, S., Tang, H., Bruening, J. M., Hofton, M. A., Blair, J. B., & Luthcke, S. B. (2022). GEDI L4A Footprint Level Aboveground Biomass Density, Version 2.1. ORNL Distributed Active Archive Center [Dataset]. https://doi.org/10.3334/ORNLDAAC/2056

European Commission,. (2021). *New EU forest strategy for 2030*. https://op.europa.eu/s/zNWR

European Environment Agency, & European Environment Agency. (2024). Forest Type 2018 - Present (raster 10m), Europe, 3-yearly, Nov. 2024 [Dataset]. European Environment Agency. https://doi.org/10.2909/77873FF3-4EDF-48D4-94CD-C5B7B61DA29E

Farquhar, G. D., von Caemmerer, S., & Berry, J. A. (1980). A biochemical model of photosynthetic CO2 assimilation in leaves of C 3 species. *Planta*, *149*(1), 78–90. https://doi.org/10.1007/BF00386231

Fattorini, L., Marcheselli, M., & Pisani, C. (2006). A three-phase sampling strategy for large-scale multiresource forest inventories. *Journal of Agricultural, Biological, and Environmental Statistics*, *11*(3), 296–316. https://doi.org/10.1198/108571106x130548

Fibbi, L., Moriondo, M., Chiesi, M., Bindi, M., & Maselli, F. (2019). Impacts of climate change on the gross primary production of Italian forests. *Annals of Forest Science*, *76*(2). https://doi.org/10.1007/s13595-019-0843-x

Fischer, R., Knapp, N., Bohn, F., Shugart, H. H., & Huth, A. (2019). The relevance of forest structure for biomass and productivity in temperate forests: New perspectives for remote sensing. *Surveys in Geophysics*, *40*(4), 709–734. https://doi.org/10.1007/s10712-019-09519-x

Flexas, J., & Medrano, H. (2002). Drought-inhibition of photosynthesis in C3 plants: stomatal

and non-stomatal limitations revisited. *Annals of Botany*, *89*(2), 183–189. https://doi.org/10.1093/aob/mcf027

Food and Agriculture Organization of the United Nations, United Nations Environment Programme, Mediterranean Action Plan Barcelona Convention, & Bleu, P. (2019). *State of Mediterranean Forests 2018*. Food & Agriculture Org. https://books.google.com/books?hl=it&lr=&id=Tmy1DwAAQBAJ&oi=fnd&pg=PR3&dq=Bleu,+P.+(2019).+State+of+Mediterranean+forests+2018.&ots=r4f-wsL3Gy&sig=EhKKvjR4J6yEpHQhlC6yL6bxbJ0

Frank, D., Reichstein, M., Bahn, M., Thonicke, K., Frank, D., Mahecha, M. D., Smith, P., van der Velde, M., Vicca, S., Babst, F., Beer, C., Buchmann, N., Canadell, J. G., Ciais, P., Cramer, W., Ibrom, A., Miglietta, F., Poulter, B., Rammig, A., … Zscheischler, J. (2015). Effects of climate extremes on the terrestrial carbon cycle: concepts, processes and potential future impacts. *Global Change Biology*, *21*(8), 2861–2880. https://doi.org/10.1111/gcb.12916

Gaber, M., Kang, Y., Schurgers, G., & Keenan, T. (2024). Using automated machine learning for the upscaling of gross primary productivity. *Biogeosciences*, *21*(10), 2447–2472. https://doi.org/10.5194/bg-21-2447-2024

Gao, B. C. (1996). NDWI--a normalized difference water index for remote sensing of vegetation liquid water from space. *Remote Sensing of Environment*, *58*(3), 257–256. https://doi.org/10.1016/s0034-4257(96)00067-3

Gasparini, P., & Tabacchi, G. (2022). Changes of Italian Forests Over Time Captured by the National Forest Inventories: L'evoluzione nel tempo delle foreste italiane secondo gli inventari forestali nazionali. In *Italian National Forest Inventory—Methods and Results of*

the Third Survey (pp. 545–568). Springer International Publishing. https://doi.org/10.1007/978-3-030-98678-0_13

Gobiet, A., Kotlarski, S., Beniston, M., Heinrich, G., Rajczak, J., & Stoffel, M. (2014). 21st century climate change in the European Alps--a review. *The Science of the Total Environment*, *493*, 1138–1151. https://doi.org/10.1016/j.scitotenv.2013.07.050

Goulden, M. L., & Bales, R. C. (2014). Mountain runoff vulnerability to increased evapotranspiration with vegetation expansion. *Proceedings of the National Academy of Sciences of the United States of America*, *111*(39), 14071–14075. https://doi.org/10.1073/pnas.1319316111

Grossiord, C., Buckley, T. N., Cernusak, L. A., Novick, K. A., Poulter, B., Siegwolf, R. T. W., Sperry, J. S., & McDowell, N. G. (2020). Plant responses to rising vapor pressure deficit. *The New Phytologist*, *226*(6), 1550–1566. https://doi.org/10.1111/nph.16485

Härkönen, S., Lehtonen, A., Eerikäinen, K., Peltoniemi, M., & Mäkelä, A. (2011). Estimating forest carbon fluxes for large regions based on process-based modelling, NFI data and Landsat satellite images. *Forest Ecology and Management*, *262*(12), 2364–2377. https://doi.org/10.1016/j.foreco.2011.08.035

Hartmann, H., Bastos, A., Das, A. J., Esquivel-Muelbert, A., Hammond, W. M., Martínez-Vilalta, J., McDowell, N. G., Powers, J. S., Pugh, T. A. M., Ruthrof, K. X., & Allen, C. D. (2022). Climate change risks to global forest health: Emergence of unexpected events of elevated tree mortality worldwide. *Annual Review of Plant Biology*, *73*(1), 673–702. https://doi.org/10.1146/annurev-arplant-102820-012804

Herrnegger, M., Nachtnebel, H.-P., & Haiden, T. (2012). Evapotranspiration in high alpine catchments – an important part of the water balance! *Hydrology Research*, *43*(4), 460–475.

https://doi.org/10.2166/nh.2012.132

Holtmann, A., Huth, A., Pohl, F., Rebmann, C., & Fischer, R. (2021). Carbon sequestration in mixed deciduous forests: The influence of tree size and species composition derived from model experiments. *Forests*, *12*(6), 726. https://doi.org/10.3390/f12060726

Hu, Z., Sun, S., Sun, X., Lin, S., Song, C., & Wang, G. (2023). Controlling factors of the spatial-temporal fluctuations in evapotranspiration along an elevation gradient across humid Montane ecosystems. *Water Resources Research*, *59*(1). https://doi.org/10.1029/2022wr033228

INFC. (2015). *Inventario Nazionale delle Foreste e dei serbatoi di Carbonio. Corpo Forestale dello Stato*. https://www.inventarioforestale.org/en/statistiche_infc/

IPCC. (2022). Summary for policymakers. In Climate change 2021: Impacts, adaptation and vulnerability. Contribution of working group 2 to the Sixth Assessment Report of the Intergovernmental Panel on Climate Change. *Cambridge University Press*.

Jarvis, P. G. (1976). The interpretation of the variations in leaf water potential and stomatal conductance found in canopies in the field. *Philosophical Transactions of the Royal Society of London*, *273*(927), 593–610. https://doi.org/10.1098/rstb.1976.0035

Jiao, J., Su, D., Han, L., & Wang, Y. (2016). A rainfall interception model for alfalfa canopy under simulated sprinkler irrigation. *Water*, *8*(12), 585. https://doi.org/10.3390/w8120585

Johansson, U., Boström, H., Löfström, T., & Linusson, H. (2014). Regression conformal prediction with random forests. *Machine Learning*, *97*(1-2), 155–176. https://doi.org/10.1007/s10994-014-5453-0

Jung, M., Reichstein, M., Margolis, H. A., Cescatti, A., Richardson, A. D., Arain, M. A., Arneth, A., Bernhofer, C., Bonal, D., Chen, J., Gianelle, D., Gobron, N., Kiely, G., Kutsch, W.,

1131 Lasslop, G., Law, B. E., Lindroth, A., Merbold, L., Montagnani, L., … Williams, C. (2011).
1132 Global patterns of land-atmosphere fluxes of carbon dioxide, latent heat, and sensible heat
1133 derived from eddy covariance, satellite, and meteorological observations. *Journal of*
1134 *Geophysical Research*, *116*(G00J07). https://doi.org/10.1029/2010jg001566
1135Kapeller, S., Lexer, M. J., Geburek, T., Hiebl, J., & Schueler, S. (2012). Intraspecific variation in
1136 climate response of Norway spruce in the eastern Alpine range: Selecting appropriate
1137 provenances for future climate. *Forest Ecology and Management*, *271*, 46–57.
1138 https://doi.org/10.1016/j.foreco.2012.01.039
1139Karimzadeh, S., Ahmadi, A., Baldocchi, D., & Fisher, J. B. (2025). Climate change has
1140 increased global evaporative demand except in South Asia. *Communications Earth &*
1141 *Environment*, *6*(1). https://doi.org/10.1038/s43247-025-02959-x
1142Kattge, J., & Knorr, W. (2007). Temperature acclimation in a biochemical model of
1143 photosynthesis: a reanalysis of data from 36 species. *Plant, Cell & Environment*, *30*(9),
1144 1176–1190. https://doi.org/10.1111/j.1365-3040.2007.01690.x
1145Kennedy, R. E., Yang, Z., & Cohen, W. B. (2010). Detecting trends in forest disturbance and
1146 recovery using yearly Landsat time series: 1. LandTrendr — Temporal segmentation
1147 algorithms. *Remote Sensing of Environment*, *114*(12), 2897–2910.
1148 https://doi.org/10.1016/j.rse.2010.07.008
1149Khadke, L., Verma, A., Mukherjee, S., & Ghosh, S. (2026). Vapor pressure deficit dominates sap
1150 flow variability across forest biomes. *Journal of Hydrology*, *664*(134449), 134449.
1151 https://doi.org/10.1016/j.jhydrol.2025.134449
1152Kingma, D. P., & Ba, J. (2014). Adam: A method for stochastic optimization. In *arXiv [cs.LG]*.
1153 arXiv. https://doi.org/10.48550/arXiv.1412.6980

1154Kotlarski, S., Gobiet, A., Morin, S., Olefs, M., Rajczak, J., & Samacoïts, R. (2022). 21st Century
1155 alpine climate change. *Climate Dynamics*. https://doi.org/10.1007/s00382-022-06303-3
1156Kozii, N., Haahti, K., Tor-ngern, P., Chi, J., Hasselquist, E. M., Laudon, H., Launiainen, S.,
1157 Oren, R., Peichl, M., Wallerman, J., & Hasselquist, N. J. (2020). Partitioning growing
1158 season water balance within a forested boreal catchment using sap flux, eddy covariance,
1159 and a process-based model. *Hydrology and Earth System Sciences*, *24*(6), 2999–3014.
1160 https://doi.org/10.5194/hess-24-2999-2020
1161Lal, R. (2005). Forest soils and carbon sequestration. *Forest Ecology and Management*, *220*(1-
1162 3), 242–258. https://doi.org/10.1016/j.foreco.2005.08.015
1163Larocque, G. R., Bhatti, J. S., Gordon, A. M., Luckai, N., Wattenbach, M., Liu, J., Peng, C., Arp,
1164 P. A., Liu, S., Zhang, C.-F., Komarov, A., Grabarnik, P., Sun, J., & White, T. (2008).
1165 Chapter eighteen uncertainty and sensitivity issues in process-based models of carbon and
1166 nitrogen cycles in terrestrial ecosystems. In *Environmental Modelling, Software and*
1167 *Decision Support* (pp. 307–327). Elsevier. https://doi.org/10.1016/s1574-101x(08)00618-2
1168Leng, J., Chen, J. M., Li, W., Luo, X., Xu, M., Liu, J., Wang, R., Rogers, C., Li, B., & Yan, Y.
1169 (2024). Global datasets of hourly carbon and water fluxes simulated using a satellite-based
1170 process model with dynamic parameterizations. *Earth System Science Data*, *16*(3), 1283–
1171 1300. https://doi.org/10.5194/essd-16-1283-2024
1172Lewińska, K. E., Ivits, E., Schardt, M., & Zebisch, M. (2018). Drought impact on phenology and
1173 green biomass production of alpine mountain forest—case study of South Tyrol 2001–2012
1174 inspected with MODIS time series. *Forests*, *9*(2), 91. https://doi.org/10.3390/f9020091
1175Liang, T., Tian, F., Zou, L., Jin, H., Tagesson, T., Rumpf, S., He, T., Liang, S., & Fensholt, R.
1176 (2024). Global assessment of vegetation patterns along topographic gradients. *International*

Journal of Digital Earth, *17*(1). https://doi.org/10.1080/17538947.2024.2404232

Liang, X., Zhang, T., Lu, X., Ellsworth, D. S., BassiriRad, H., You, C., Wang, D., He, P., Deng, Q., Liu, H., Mo, J., & Ye, Q. (2020). Global response patterns of plant photosynthesis to nitrogen addition: A meta-analysis. *Global Change Biology*, *26*(6), 3585–3600. https://doi.org/10.1111/gcb.15071

Liu, Q., Zhang, T., Du, M., Gao, H., Zhang, Q., & Sun, R. (2022). A better carbon-water flux simulation in multiple vegetation types by data assimilation. *Forest Ecosystems*, *9*(100013), 100013. https://doi.org/10.1016/j.fecs.2022.100013

Lorenz, K., & Lal, R. (2009). *Carbon sequestration in forest ecosystems* (2010th ed.) [PDF]. Springer. https://doi.org/10.1007/978-90-481-3266-9

Luo, Y., Liu, D., Fu, B., Huang, C., Fan, J., & Shao, X. (2026). Scale-dependent effects of forest spatial structure on gross primary productivity across China. *Frontiers in Forests and Global Change*, *9*(1825611). https://doi.org/10.3389/ffgc.2026.1825611

Luo, Z., Ren, J., Zhuang, Q., & Fatichi, S. (2026). Transpiration changes with soil warming: Insights from a mechanistic model. *Geophysical Research Letters*, *53*(8). https://doi.org/10.1029/2025gl120046

Mahnken, M., Cailleret, M., Collalti, A., Trotta, C., Biondo, C., D'Andrea, E., Dalmonech, D., Marano, G., Mäkelä, A., Minunno, F., Peltoniemi, M., Trotsiuk, V., Nadal-Sala, D., Sabaté, S., Vallet, P., Aussenac, R., Cameron, D. R., Bohn, F. J., Grote, R., … Reyer, C. P. O. (2022). Accuracy, realism and general applicability of European forest models. *Global Change Biology*, *28*(23), 6921–6943. https://doi.org/10.1111/gcb.16384

Marconi, S., Chiti, T., Nolè, A., Valentini, R., & Collalti, A. (2017). The role of respiration in estimation of net carbon cycle: Coupling soil carbon dynamics and canopy turnover in a

novel version of 3D-CMCC forest ecosystem model. *Forests*, *8*(6), 220. https://doi.org/10.3390/f8060220

Maxwell, A. E., Warner, T. A., & Fang, F. (2018). Implementation of machine-learning classification in remote sensing: an applied review. *International Journal of Remote Sensing*, *39*(9), 2784–2817. https://doi.org/10.1080/01431161.2018.1433343

Medlyn, B. E., Dreyer, E., Ellsworth, D., Forstreuter, M., Harley, P. C., Kirschbaum, M. U. F., Le Roux, X., Montpied, P., Strassemeyer, J., Walcroft, A., Wang, K., & Loustau, D. (2002). Temperature response of parameters of a biochemically based model of photosynthesis. II. A review of experimental data: Temperature response of photosynthetic parameters - review. *Plant, Cell & Environment*, *25*(9), 1167–1179. https://doi.org/10.1046/j.1365-3040.2002.00891.x

Mehmood, K., Anees, S. A., Rehman, A., Rehman, N. U., Muhammad, S., Shahzad, F., Liu, Q., Alharbi, S. A., Alfarraj, S., Ansari, M. J., & Khan, W. R. (2024). Assessment of climatic influences on net primary productivity along elevation gradients in temperate ecoregions. *Trees, Forests and People*, *18*(100657), 100657. https://doi.org/10.1016/j.tfp.2024.100657

Mehrotra, K., Mohan, C. K., & Ranka, S. (1997). *Elements of artificial neural networks*. https://www.academia.edu/download/54062107/Elements_of_Artificial_Neural_Nets20170804-2600-1uzz5ca.pdf

Ménégoz, M., Valla, E., Jourdain, N. C., Blanchet, J., Beaumet, J., Wilhelm, B., Gallée, H., Fettweis, X., Morin, S., & Anquetin, S. (2020). Contrasting seasonal changes in total and intense precipitation in the European Alps from 1903 to 2010. *Hydrology and Earth System Sciences*, *24*(11), 5355–5377. https://doi.org/10.5194/hess-24-5355-2020

Migliavacca, M., Musavi, T., Mahecha, M. D., Nelson, J. A., Knauer, J., Baldocchi, D. D.,

1223 Perez-Priego, O., Christiansen, R., Peters, J., Anderson, K., Bahn, M., Black, T. A.,
1224 Blanken, P. D., Bonal, D., Buchmann, N., Caldararu, S., Carrara, A., Carvalhais, N.,
1225 Cescatti, A., … Reichstein, M. (2021). The three major axes of terrestrial ecosystem
1226 function. *Nature*, *598*(7881), 468–472. https://doi.org/10.1038/s41586-021-03939-9
1227 Molotch, N. P., Brooks, P. D., Burns, S. P., Litvak, M., Monson, R. K., McConnell, J. R., &
1228 Musselman, K. (2009). Ecohydrological controls on snowmelt partitioning in mixed-conifer
1229 sub-alpine forests. *Ecohydrology: Ecosystems, Land and Water Process Interactions, Ecohydrogeomorphology*, *2*(2), 129–142. https://doi.org/10.1002/eco.48
1231 Monteith, J., & Unsworth, M. (2007). *Principles of environmental physics* (3rd ed.). Academic
1232 Press. https://booksite.elsevier.com/samplechapters/9780125051033/Sample_Chapters/
1233 01~Front_Matter.pdf
1234 Morales, P., Sykes, M. T., Prentice, I. C., Smith, P., Smith, B., Bugmann, H., Zierl, B.,
1235 Friedlingstein, P., Viovy, N., Sabaté, S., Sánchez, A., Pla, E., Gracia, C. A., Sitch, S.,
1236 Arneth, A., & Ogee, J. (2005). Comparing and evaluating process-based ecosystem model
1237 predictions of carbon and water fluxes in major European forest biomes. *Global Change Biology*, *11*(12), 2211–2233. https://doi.org/10.1111/j.1365-2486.2005.01036.x
1239 Morichetti, M., Vangi, E., & Collalti, A. (2024). Predicted future changes in the mean seasonal
1240 carbon cycle due to climate change. *Forests*, *15*(7), 1124.
1241 https://doi.org/10.3390/f15071124
1242 Motta, R., Ascoli, D., Corona, P., Marchetti, M., & Vacchiano, G. (2018). Silviculture and wind
1243 damages. The storm “Vaia.” *Forest@*, *15*(1), 94–98. https://doi.org/10.3832/efor2990-015
1244 Niu, Z., He, H., Peng, S., Ren, X., Zhang, L., Gu, F., Zhu, G., Peng, C., Li, P., Wang, J., Ge, R.,
1245 Zeng, N., Zhu, X., Lv, Y., Chang, Q., Xu, Q., Zhang, M., & Liu, W. (2021). A process-

based model integrating remote sensing data for evaluating ecosystem services. *Journal of Advances in Modeling Earth Systems*, *13*(6). https://doi.org/10.1029/2020ms002451

Olden, J. D., Lawler, J. J., & Poff, N. L. (2008). Machine learning methods without tears: a primer for ecologists. *The Quarterly Review of Biology*, *83*(2), 171–193. https://doi.org/10.1086/587826

Pagano, A., Amato, F., Ippolito, M., De Caro, D., Croce, D., Motisi, A., Provenzano, G., & Tinnirello, I. (2023). Machine learning models to predict daily actual evapotranspiration of citrus orchards under regulated deficit irrigation. *Ecological Informatics*, *76*(102133), 102133. https://doi.org/10.1016/j.ecoinf.2023.102133

Pal, M., & Mather, P. M. (2005). Support vector machines for classification in remote sensing. *International Journal of Remote Sensing*, *26*(5), 1007–1011. https://doi.org/10.1080/01431160512331314083

Paris Climate Agreement. (2015). *Paris Climate Agreement*. https://unfccc.int/sites/default/file/english_paris_agreement.pdf

Piao, S., Friedlingstein, P., Ciais, P., Viovy, N., & Demarty, J. (2007). Growing season extension and its impact on terrestrial carbon cycle in the Northern Hemisphere over the past 2 decades. *Global Biogeochemical Cycles*, *21*(3). https://doi.org/10.1029/2006gb002888

Ploton, P., Mortier, F., Réjou-Méchain, M., Barbier, N., Picard, N., Rossi, V., Dormann, C., Cornu, G., Viennois, G., Bayol, N., Lyapustin, A., Gourlet-Fleury, S., & Pélissier, R. (2020). Spatial validation reveals poor predictive performance of large-scale ecological mapping models. *Nature Communications*, *11*(1), 4540. https://doi.org/10.1038/s41467-020-18321-y

Poon, P. K., & Kinoshita, A. M. (2018). Estimating evapotranspiration in a post-fire environment

using remote sensing and machine learning. *Remote Sensing*, *10*(11), 1728. https://doi.org/10.3390/rs10111728

Pulliainen, J., Aurela, M., Laurila, T., Aalto, T., Takala, M., Salminen, M., Kulmala, M., Barr, A., Heimann, M., Lindroth, A., Laaksonen, A., Derksen, C., Mäkelä, A., Markkanen, T., Lemmetyinen, J., Susiluoto, J., Dengel, S., Mammarella, I., Tuovinen, J.-P., & Vesala, T. (2017). Early snowmelt significantly enhances boreal springtime carbon uptake. *Proceedings of the National Academy of Sciences of the United States of America*, *114*(42), 11081–11086. https://doi.org/10.1073/pnas.1707889114

Rank, P. H., Vaghasiya, D. R., Lunagaria, M. M., Patel, R. J., Tiwari, M. K., & Rank, H. D. (2023). Climate change impacts on water flux dynamics in Shingoda basin having agriculture and forest ecosystems: A comprehensive analysis. *Journal of Agrometeorology*, *25*(3). https://doi.org/10.54386/jam.v25i3.2284

Richardson, A. D., Hollinger, D. Y., Dail, D. B., Lee, J. T., Munger, J. W., & O'keefe, J. (2009). Influence of spring phenology on seasonal and annual carbon balance in two contrasting New England forests. *Tree Physiology*, *29*(3), 321–331. https://doi.org/10.1093/treephys/tpn040

Roberts, D. R., Bahn, V., Ciuti, S., Boyce, M. S., Elith, J., Guillera-Arroita, G., Hauenstein, S., Lahoz-Monfort, J. J., Schröder, B., Thuiller, W., Warton, D. I., Wintle, B. A., Hartig, F., & Dormann, C. F. (2017). Cross-validation strategies for data with temporal, spatial, hierarchical, or phylogenetic structure. *Ecography*, *40*(8), 913–929. https://doi.org/10.1111/ecog.02881

Roxburgh, S. H., Berry, S. L., Buckley, T. N., Barnes, B., & Roderick, M. L. (2005). What is NPP? Inconsistent accounting of respiratory fluxes in the definition of net primary

production. *Functional Ecology*, *19*(3), 378–382. https://doi.org/10.1111/j.1365-2435.2005.00983.x

Ryan, M. G., Binkley, D., & Fownes, J. H. (1997). Age-related decline in forest productivity: Pattern and process. In *Advances in Ecological Research Volume 27* (pp. 213–262). Elsevier. https://doi.org/10.1016/s0065-2504(08)60009-4

Ryan, M. G., & Yoder, B. J. (1997). Hydraulic limits to tree height and tree growth. *Bioscience*, *47*(4), 235–242. https://doi.org/10.2307/1313077

Saponaro, V., De Cáceres, M., Dalmonech, D., D'Andrea, E., Vangi, E., & Collalti, A. (2025). Assessing the combined effects of forest management and climate change on carbon and water fluxes in European beech forests. *Forest Ecosystems*, *12*(100290), 100290. https://doi.org/10.1016/j.fecs.2024.100290

Schlesinger, W. H., & Jasechko, S. (2014). Transpiration in the global water cycle. *Agricultural and Forest Meteorology*, *189-*, 115–117. https://doi.org/10.1016/j.agrformet.2014.01.011

Schönbeck, L. C., Schuler, P., Lehmann, M. M., Mas, E., Mekarni, L., Pivovaroff, A. L., Turberg, P., & Grossiord, C. (2022). Increasing temperature and vapour pressure deficit lead to hydraulic damages in the absence of soil drought. *Plant, Cell & Environment*, *45*(11), 3275–3289. https://doi.org/10.1111/pce.14425

Schulzweida, U. (2023). *CDO User Guide*. Zenodo. https://doi.org/10.5281/ZENODO.10020800

Sheil, D. (2018). Forests, atmospheric water and an uncertain future: the new biology of the global water cycle. *Forest Ecosystems*, *5*(1). https://doi.org/10.1186/s40663-018-0138-y

Shiklomanov, A. N., Bond-Lamberty, B., Atkins, J. W., & Gough, C. M. (2020). Structure and parameter uncertainty in centennial projections of forest community structure and carbon cycling. *Global Change Biology*, *26*(11), 6080–6096. https://doi.org/10.1111/gcb.15164

Shumway, R. H., & Stoffer, D. S. (2017). *Time series analysis and its applications* (4th ed.) [PDF]. Springer International Publishing. https://doi.org/10.1007/978-3-319-52452-8

Smith, N. G., & Dukes, J. S. (2013). Plant respiration and photosynthesis in global-scale models: incorporating acclimation to temperature and CO2. *Global Change Biology*, *19*(1), 45–63. https://doi.org/10.1111/j.1365-2486.2012.02797.x

Strasser, U., Warscher, M., Rottler, E., & Hanzer, F. (2024). openAMUNDSEN v1.0: an open-source snow-hydrological model for mountain regions. *Geoscientific Model Development*, *17*(17), 6775–6797. https://doi.org/10.5194/gmd-17-6775-2024

Sulman, B. N., Roman, D. T., Yi, K., Wang, L., Phillips, R. P., & Novick, K. A. (2016). High atmospheric demand for water can limit forest carbon uptake and transpiration as severely as dry soil: VPD CONTROL OF GPP AND TRANSPIRATION. *Geophysical Research Letters*, *43*(18), 9686–9695. https://doi.org/10.1002/2016gl069416

Sun, Y., Guan, Q., Du, Q., Wang, Q., & Sun, W. (2025). Elevation dependence of vegetation growth stages and carbon sequestration dynamics in high mountain ecosystems. *Environmental Research*, *273*(121200), 121200. https://doi.org/10.1016/j.envres.2025.121200

Tabacchi, G., Di Cosmo, L., Gasparini, P., & Morelli, S. (2011). *Stima del volume e della fitomassa delle principali specie forestali italiane*. Consiglio per la Ricerca e la sperimentazione in Agricoltura. https://www.inventarioforestale.org/wp-content/uploads/2022/10/tavole_cubatura.pdf

Taquet, V., Blot, V., Morzadec, T., Lacombe, L., & Brunel, N. (2022). MAPIE: an open-source library for distribution-free uncertainty quantification. In *arXiv [stat.ML]*. arXiv. https://doi.org/10.48550/arXiv.2207.12274

Tarquini, S., Isola, I., Favalli, M., Mazzarini, F., Bisson, M., Pareschi, M. T., & Boschi, E. (2007). TINITALY/01: a new Triangular Irregular Network of Italy [Dataset]. Annals of Geophysics, 50(3), 407–425. https://doi.org/10.4401/ag-4424

Tetens, O. (1930). Uber einige meteorologische begriffe. *Z. Geophys*, *6*, 297–309. https://www.semanticscholar.org/paper/Uber-einige-meteorologische-begriffe-Tetens/33b71d32374b7572d1399fcac74ef7fb9a40a9ef

Thornthwaite, C. W., & Mather, J. R. (1951). The role of evapotranspiration in climate. *Archiv Für Meteorologie, Geophysik Und Bioklimatologie Serie B*, *3*(1), 16–39. https://doi.org/10.1007/bf02242588

Tian, Z., Fu, Y., Zhou, T., Yi, C., Kutter, E., Zhang, Q., & Krakauer, N. Y. (2024). Estimating forest gross primary production using machine learning, light use efficiency model, and global eddy covariance data. *Forests*, *15*(9), 1615. https://doi.org/10.3390/f15091615

Tolan, J., Yang, H.-I., Nosarzewski, B., Couairon, G., Vo, H. V., Brandt, J., Spore, J., Majumdar, S., Haziza, D., Vamaraju, J., Moutakanni, T., Bojanowski, P., Johns, T., White, B., Tiecke, T., & Couprie, C. (2024). Very high resolution canopy height maps from RGB imagery using self-supervised vision transformer and convolutional decoder trained on aerial lidar [Dataset]. Remote Sensing of Environment, 300(113888), 113888. https://doi.org/10.1016/j.rse.2023.113888

Trotsiuk, V., Hartig, F., Cailleret, M., Babst, F., Forrester, D. I., Baltensweiler, A., Buchmann, N., Bugmann, H., Gessler, A., Gharun, M., Minunno, F., Rigling, A., Rohner, B., Stillhard, J., Thürig, E., Waldner, P., Ferretti, M., Eugster, W., & Schaub, M. (2020). Assessing the response of forest productivity to climate extremes in Switzerland using model-data fusion. *Global Change Biology*, *26*(4), 2463–2476. https://doi.org/10.1111/gcb.15011

Urban, A., & Urban, J. (2024). A decline in stomatal conductance is the primary reason for low photosynthesis in veteran pedunculate oak trees. *Forests*, *15*(12), 2118. https://doi.org/10.3390/f15122118

Valentini, R., & Miglietta, F. (2014). *The greenhouse gas balance of Italy; An insight on managed and natural terrestrial ecosystems: An insight on managed and natural terrestrial ecosystems* (R. Valentini & F. Miglietta (eds.); 2015th ed.) [PDF]. Springer. https://doi.org/10.1007/978-3-642-32424-6

van der Woude, A. M., Peters, W., Joetzjer, E., Lafont, S., Koren, G., Ciais, P., Ramonet, M., Xu, Y., Bastos, A., Botía, S., Sitch, S., de Kok, R., Kneuer, T., Kubistin, D., Jacotot, A., Loubet, B., Herig-Coimbra, P.-H., Loustau, D., & Luijkx, I. T. (2023). Temperature extremes of 2022 reduced carbon uptake by forests in Europe. *Nature Communications*, *14*(1), 6218. https://doi.org/10.1038/s41467-023-41851-0

Vangi, E., Dalmonech, D., d'Amico, G., Grieco, E., Morichetti, M., Puchi, P. F., Francini, S., Fares, S., Giannetti, F., Corona, P., Barbetti, R., Chirici, G., & Collalti, A. (2025). Monitoring forest attributes, C-fluxes, and C-stocks using the process-based model 3D-CMCC-FEM at the National level. *Ecological Informatics*, *92*(103489), 103489. https://doi.org/10.1016/j.ecoinf.2025.103489

Vangi, E., Dalmonech, D., Morichetti, M., Grieco, E., Giannetti, F., D'Amico, G., Nakhavali, M. (andre), Chirici, G., & Collalti, A. (2024). Stand age and climate change effects on carbon increments and stock dynamics. *Forests*, *15*(7), 1120. https://doi.org/10.3390/f15071120

Vangi, E., D'Amico, G., Saponaro, V., Niccoli, M., Tiberi, G., Francini, S., Borghi, C., Collalti, A., Parisi, F., & Chirici, G. (2026). Investigating climate-phenology relationships among the most common Italian forest species using Sentinel-2-derived vegetation phenology and

productivity products. In *bioRxiv*. bioRxiv. https://doi.org/10.64898/2026.02.23.707431

Vovk, V. (2012). Cross-conformal predictors. In *arXiv [stat.ML]*. arXiv. https://doi.org/10.48550/arXiv.1208.0806

Wang, J., Hua, H., Guo, J., Huang, X., Zhang, X., Yang, Y., Wang, D., Guo, X., Zhang, R., Smith, N. G., Rossi, S., Peñuelas, J., Ciais, P., Wu, C., & Chen, L. (2025). Late spring frost delays tree spring phenology by reducing photosynthetic productivity. *Nature Climate Change*, *15*(2), 201–209. https://doi.org/10.1038/s41558-024-02205-w

Wang, X., Wang, T., Guo, H., Liu, D., Zhao, Y., Zhang, T., Liu, Q., & Piao, S. (2018). Disentangling the mechanisms behind winter snow impact on vegetation activity in northern ecosystems. *Global Change Biology*, *24*(4), 1651–1662. https://doi.org/10.1111/gcb.13930

Wang, Y., Xiao, P., Zhang, X., Liu, H., Wu, Y., & Sun, L. (2024). Unraveling the effects of snow cover change on vegetation productivity: Insights from underlying surface types. *Ecosphere (Washington, D.C)*, *15*(5). https://doi.org/10.1002/ecs2.4855

Waring, R. H., & Running, S. W. (2007). Forest ecosystem analysis at multiple time and space scales. In *Forest Ecosystems* (pp. 1–16). Elsevier. https://doi.org/10.1016/b978-012370605-8.50005-0

Wen, R., Qin, M., Jiang, P., Yang, F., Liu, B., Zhu, M., Fang, Y., Tian, Y., & Shang, B. (2024). Vegetation and evapotranspiration responses to increased atmospheric vapor pressure deficit across the global forest. *Atmosphere*, *15*(4), 408. https://doi.org/10.3390/atmos15040408

West, P. W. (2020). Do increasing respiratory costs explain the decline with age of forest growth rate? *Journal of Forestry Research*, *31*(3), 693–712. https://doi.org/10.1007/s11676-019-01020-w

1407Wetzel, P. J., & Chang, J.-T. (1987). Concerning the relationship between evapotranspiration and
1408 soil moisture. *Journal of Climate and Applied Meteorology*, *26*(1), 18–27.
1409 https://doi.org/10.1175/1520-0450(1987)026<0018:ctrbea>2.0.co;2
1410Whitehead, D. (1998). Regulation of stomatal conductance and transpiration in forest canopies.
1411 *Tree Physiology*, *18*(8_9), 633–644. https://doi.org/10.1093/treephys/18.8-9.633
1412White, J. C., Wulder, M. A., Hobart, G. W., Luther, J. E., Hermosilla, T., Griffiths, P., Coops, N.
1413 C., Hall, R. J., Hostert, P., Dyk, A., & Guindon, L. (2014). Pixel-based image compositing
1414 for large-area dense time series applications and science. *Canadian Journal of Remote*
1415 *Sensing/Journal Canadien de Teledetection*, *40*(3), 192–212.
1416 https://doi.org/10.1080/07038992.2014.945827
1417Wortman, E., Tomaszewski, T., Waldner, P., Schleppi, P., Thimonier, A., Eugster, W.,
1418 Buchmann, N., & Sievering, H. (2012). Atmospheric nitrogen deposition and canopy
1419 retention influences on photosynthetic performance at two high nitrogen deposition Swiss
1420 forests. *Tellus. Series B, Chemical and Physical Meteorology*, *64*(1), 17216. https://doi.org/
1421 10.3402/tellusb.v64i0.17216
1422Xu, T., Guo, Z., Liu, S., He, X., Meng, Y., Xu, Z., Xia, Y., Xiao, J., Zhang, Y., Ma, Y., & Song,
1423 L. (2018). Evaluating different machine learning methods for upscaling evapotranspiration
1424 from flux towers to the regional scale. *Journal of Geophysical Research. Atmospheres:*
1425 *JGR*, *123*(16), 8674–8690. https://doi.org/10.1029/2018jd028447
1426Yamori, W., Hikosaka, K., & Way, D. A. (2014). Temperature response of photosynthesis in C3,
1427 C4, and CAM plants: temperature acclimation and temperature adaptation. *Photosynthesis*
1428 *Research*, *119*(1-2), 101–117. https://doi.org/10.1007/s11120-013-9874-6
1429Yang, Y., Roderick, M. L., Guo, H., Miralles, D. G., Zhang, L., Fatichi, S., Luo, X., Zhang, Y.,

McVicar, T. R., Tu, Z., Keenan, T. F., Fisher, J. B., Gan, R., Zhang, X., Piao, S., Zhang, B., & Yang, D. (2023). Evapotranspiration on a greening earth. *Nature Reviews. Earth & Environment*, *4*(9), 626–641. https://doi.org/10.1038/s43017-023-00464-3

Yan, W., Zhong, Y., & Shangguan, Z. (2016). A meta-analysis of leaf gas exchange and water status responses to drought. *Scientific Reports*, *6*(1), 20917. https://doi.org/10.1038/srep20917

Zhang, J., Nielsen, S. E., Mao, L., Chen, S., Svenning, J.-C., & McGlone, M. (2016). Regional and historical factors supplement current climate in shaping global forest canopy height. *The Journal of Ecology*, *104*(2), 469–478. https://doi.org/10.1111/1365-2745.12510

Zhang, Q., Yang, X., Ding, C., Xiu, W., Liu, C., & Dai, S. (2025). Optimization of sensor combinations for simplified estimation of reference crop evapotranspiration using machine learning and SHAP interpretation. *Agriculture*, *16*(1), 93. https://doi.org/10.3390/agriculture16010093

Zhang, Y., Ma, J., Liang, S., Li, X., & Li, M. (2020). An evaluation of eight machine learning regression algorithms for forest aboveground biomass estimation from multiple satellite data products. *Remote Sensing*, *12*(24), 4015. https://doi.org/10.3390/rs12244015

Zhao, W., Tan, W., & Li, S. (2021). High leaf area index inhibits net primary production in global temperate forest ecosystems. *Environmental Science and Pollution Research International*, *28*(18), 22602–22611. https://doi.org/10.1007/s11356-020-11928-0

Zhu, H. D., Shi, Z. H., Fang, N. F., Wu, G. L., Guo, Z. L., & Zhang, Y. (2014). Soil moisture response to environmental factors following precipitation events in a small catchment. *Catena*, *120*, 73–80. https://doi.org/10.1016/j.catena.2014.04.003

Ryan, M. G., Phillips, N., & Bond, B. J. (2006). The hydraulic limitation hypothesis revisited. *Plant, Cell & Environment*, *29*(3), 367–381.

References From the Supporting Information

Amthor, J. (2000). The McCree–de Wit–penning de Vries–Thornley respiration paradigms: 30 years later. Annals of Botany, 86(1), 1–20. https://doi.org/10.1006/anbo.2000.1175

Collalti, A., Dalmonech, D., Vangi, E., Marano, G., Puchi, P. F., Morichetti, M., Saponaro, V., Orrico, M. R., & Grieco, E. (2024). Monitoring and Predicting Forest Growth and Dynamics. CNR Edizioni. https://doi.org/10.32018/ForModLab-book-2024

Collalti, A., Perugini, L., Santini, M., Chiti, T., Nolè, A., Matteucci, G., & Valentini, R. (2014). A process-based model to simulate growth in forests with complex structure: Evaluation and use of 3D-CMCC Forest Ecosystem Model in a deciduous forest in Central Italy. Ecological Modelling, 272, 362–378. https://doi.org/10.1016/j.ecolmodel.2013.09.016

de Pury, D. G. G., & Farquhar, G. D. (1997). Simple scaling of photosynthesis from leaves to canopies without the errors of big-leaf models. Plant, Cell & Environment, 20(5), 537–557. https://doi.org/10.1111/j.1365-3040.1997.00094.x

Farquhar, G. D., von Caemmerer, S., & Berry, J. A. (1980). A biochemical model of photosynthetic CO2 assimilation in leaves of C 3 species. Planta, 149(1), 78–90. https://doi.org/10.1007/BF00386231

Jarvis, P. G. (1976). The interpretation of the variations in leaf water potential and stomatal conductance found in canopies in the field. Philosophical Transactions of the Royal Society of London, 273(927), 593–610. https://doi.org/10.1098/rstb.1976.0035

Jiao, J., Su, D., Han, L., & Wang, Y. (2016). A rainfall interception model for alfalfa canopy

under simulated sprinkler irrigation. Water, 8(12), 585. https://doi.org/10.3390/w8120585

Kattge, J., & Knorr, W. (2007). Temperature acclimation in a biochemical model of photosynthesis: a reanalysis of data from 36 species. Plant, Cell & Environment, 30(9), 1176–1190. https://doi.org/10.1111/j.1365-3040.2007.01690.x

Monteith, J., & Unsworth, M. (2007). Principles of environmental physics (3rd ed.). Academic Press. https://booksite.elsevier.com/samplechapters/9780125051033/Sample_Chapters/01~Front_Matter.pdf

Smith, N. G., & Dukes, J. S. (2013). Plant respiration and photosynthesis in global-scale models: incorporating acclimation to temperature and CO2. Global Change Biology, 19(1), 45–63. https://doi.org/10.1111/j.1365-2486.2012.02797.x

Waring, R. H., & Running, S. W. (2007). Forest ecosystem analysis at multiple time and space scales. In Forest Ecosystems (pp. 1–16). Elsevier. https://doi.org/10.1016/b978-012370605-8.50005-0